ORIGINAL RESEARCH

MK2-Deficient Mice Are Bradycardic and Display Delayed Hypertrophic Remodeling in Response to a Chronic Increase in Afterload

Matthieu Ruiz [iD], PhD; Maya Khairallah, PhD; Dharmendra Dingar, PhD; George Vaniotis, PhD; Ramzi J. Khairallah [iD], PhD; Benjamin Lauzier [iD], PhD; Simon Thibault, BSc; Joëlle Trépanier [iD], MSc; Yanfen Shi, MD; Annie Douillette, MSc; Bahira Hussein, MSc; Sherin Ali Nawaito [iD], MD, MSc, PhD; Pramod Sahadevan [iD], PhD; Albert Nguyen, PhD; Fatiha Sahmi, PhD; Marc-Antoine Gillis, MSc; Martin G. Sirois, PhD; Matthias Gaestel [iD], PhD; William C. Stanley, PhD; Céline Fiset [iD], PhD; Jean-Claude Tardif, MD; Bruce G. Allen [iD], PhD

BACKGROUND: Mitogen-activated protein kinase–activated protein kinase-2 (MK2) is a protein serine/threonine kinase activated by p38α/β. Herein, we examine the cardiac phenotype of pan MK2-null (MK2$^{-/-}$) mice.

METHODS AND RESULTS: Survival curves for male MK2$^{+/+}$ and MK2$^{-/-}$ mice did not differ (Mantel-Cox test, P=0.580). At 12 weeks of age, MK2$^{-/-}$ mice exhibited normal systolic function along with signs of possible early diastolic dysfunction; however, aging was not associated with an abnormal reduction in diastolic function. Both R-R interval and P-R segment durations were prolonged in MK2-deficient mice. However, heart rates normalized when isolated hearts were perfused ex vivo in working mode. Ca^{2+} transients evoked by field stimulation or caffeine were similar in ventricular myocytes from MK2$^{+/+}$ and MK2$^{-/-}$ mice. MK2$^{-/-}$ mice had lower body temperature and an age-dependent reduction in body weight. mRNA levels of key metabolic genes, including *Ppargc1a*, *Acadm*, *Lipe*, and *Ucp3,* were increased in hearts from MK2$^{-/-}$ mice. For equivalent respiration rates, mitochondria from MK2$^{-/-}$ hearts showed a significant decrease in Ca^{2+} sensitivity to mitochondrial permeability transition pore opening. Eight weeks of pressure overload increased left ventricular mass in MK2$^{+/+}$ and MK2$^{-/-}$ mice; however, after 2 weeks the increase was significant in MK2$^{+/+}$ but not MK2$^{-/-}$ mice. Finally, the pressure overload–induced decrease in systolic function was attenuated in MK2$^{-/-}$ mice 2 weeks, but not 8 weeks, after constriction of the transverse aorta.

CONCLUSIONS: Collectively, these results implicate MK2 in (1) autonomic regulation of heart rate, (2) cardiac mitochondrial function, and (3) the early stages of myocardial remodeling in response to chronic pressure overload.

Key Words: bradycardia ■ cardiac remodeling ■ mitochondrial permeability transition pore ■ MK2 ■ p38 MAPK

T he primary response of the heart to increased workload, especially in reaction to pressure or volume overload, is to adapt myocyte size in an attempt to reduce ventricular wall stress and compensate for increased hemodynamic demand.[1] However, unlike physiological hypertrophy, in response to exercise or during postnatal growth, stress stimuli such as arterial hypertension or myocardial infarction[1] leads to pathological hypertrophy or hypertrophic cardiomyopathy, associated with interstitial fibrosis and reexpression of a fetal gene program, which can result in increased myocardial stiffness and reduced cardiac output.[2–4] Although cardiac

CLINICAL PERSPECTIVE

What Is New?

- The effects of mitogen-activated protein kinase-activated protein kinase 2 (MK2) deficiency on cardiac structure, function, and hypertrophic remodeling were assessed using a constitutive, pan MK2-null mouse model.
- MK2 deficiency did not affect survival up to 100 weeks of age but was associated with progressive weight loss in aged mice, altered autonomic regulation of heart rate, and delayed hypertrophic remodeling in response to increased afterload.
- The expression of key metabolic genes was increased, and the Ca^{2+} sensitivity for mitochondrial permeability transition pore opening was decreased, in hearts from MK2-deficient mice.

What Are the Clinical Implications?

- Our findings suggest a role for MK2 in regulating both heart rate and mitochondrial function.
- Further studies should clarify if MK2 inhibition serves a cardioprotective effect.

Nonstandard Abbreviations and Acronyms

E	early diastolic transmitral filling velocity
MAPK	mitogen-activated protein kinase
MK2	mitogen-activated protein kinase–activated protein kinase-2
MKK3	mitogen-activated protein kinase kinase 3
mPTP	mitochondrial permeability transition pore
PGC-1α	peroxisome proliferator-activated receptor γ coactivator 1-α
TAC	transverse aortic constriction

hypertrophy is seen as a compensatory phenomenon to normalize myocardial wall stress, when sustained, cardiac hypertrophy predisposes to sudden cardiac death, arrhythmia, and development of heart failure.[5] Hence, understanding the basic signaling pathways involved in maintaining optimal cardiac function and their role in pressure overload–induced hypertrophy, as well as the associated contractile dysfunction, is necessary for the development of more effective means of prevention and treatment.

Several signaling pathways have been implicated in the transition from compensated hypertrophy to decompensated heart failure, including the mitogen-activated protein kinase (MAPK) pathway[6] in which p38 MAPK plays a central role.[7] Increased activation of p38 MAPK has been observed in both experimental and human heart failure.[8–11] However, the pathological cardiac phenotype associated with p38 MAPK signaling is, to some extent, confusing. The literature contains seemingly contradictory reports indicating that p38 activation is both beneficial and detrimental during hypertrophy. Four isoforms of p38 MAPK (p38α, p38β, p38δ, and p38γ) are expressed in the heart[12,13]: p38α and p38β have been shown to be activated during pressure overload, and this activation correlates with ventricular hypertrophy.[14,15] Similarly, p38γ and p38δ have been shown to mediate hypertrophy in response to angiotensin II infusion.[16] Furthermore, in isolated cardiomyocytes, activation of p38 using either pharmacological or genetic approaches also suggests that p38 activation is prohypertrophic.[14,17] The latter is reinforced by the attenuation of the hypertrophic response, evoked with phenylephrine or endothelin-1, using inhibitors of p38.[17] In contrast, chronic inhibition of p38 signaling using dominant-negative p38α or p38β is associated with enhanced cardiac hypertrophy in response to pressure overload or following infusion with angiotensin II, isoproterenol, or phenylephrine.[18,19] Similarly, cardiomyocyte-targeted deletion of p38α in mice did not impede hypertrophy in response to aortic banding, but increased both myocyte apoptosis and fibrosis while decreasing in cardiac contractility.[20] In contrast, myocyte-targeted activation of p38α in adult mice induced hypertrophy, fibrosis, and mortality within 1 week.[21]

Although there are divergent results, all convey a similar message, in which p38 MAPK signaling is essential for heart function and plays an important role in the pathogenesis of heart failure. However, the apparent opposing and divergent role for p38, as well as its numerous targets/substrates that are involved in a wide variety of cellular processes,[7,22] makes it difficult to predict the impact of p38 inhibition in clinical trials. Moreover, none of the p38 inhibitors developed to date translated into safe and effective clinical strategies with low and acceptable toxicity because of their unwanted systemic side effects, which include hepatotoxicity, neurotoxicity, and cardiotoxicity.[23–25] Hence, further research to better understand the role of p38 MAPK signaling in the healthy heart, especially with regards to its downstream targets, is essential to elucidate the potential therapeutic implications of targeting this signaling pathway. Over the past decade, many studies have focused on MK2, among other downstream p38 targets. Several reports suggested that targeting MK2 could lead to beneficial effects equivalent to those obtained when directly inhibiting p38 but with the additional advantage of lacking the side effects associated to p38 inhibitors[26] and could therefore serve as a potential therapeutic target. Indeed, the side effects associated with p38 inhibitors

were recently attributed to the loss of feedback control of upstream TAB1/TAK1 signaling, which in turn leads to sustained activation of proinflammatory pathways.[27,28] In contrast, this feedback control is maintained when using MK2 inhibitors, thereby preventing collateral activation of proinflammatory pathways.[29] In addition, evidence suggests that MK2 may be an interesting target in other forms of cardiomyopathy.[30] In fact, MK2 deficiency protects against ischemia-reperfusion injury.[31] Streicher et al[21] also reported that deleting MK2 in a conditional and cardiomyocyte-specific mouse model expressing constitutively active MAPK kinase 3 (MKK3) bE significantly reduces the MKK3bE-induced hypertrophy, improves contractile performance, and rescues lethality. In addition, pharmacological inhibition of MK2 reduces cardiac fibrosis and preserves cardiac function following myocardial infarction.[32] Finally, we have recently shown that the absence of MK2 prevents diabetes mellitus–induced cardiac dysfunction and perturbations in lipid metabolism.[30,33]

To date, few studies have examined the role of MK2 in either the healthy heart or in myocardial remodeling in response to a chronic increase in cardiac afterload. Therefore, using a previously described MK2-deficient mouse model,[34] this study was undertaken to investigate (1) whether MK2 is involved in maintaining basal cardiac function and (2) whether MK2 plays a role in cardiac remodeling resulting from chronic pressure overload, in which case it would represent a potential therapeutic target.

METHODS

The data that support the findings of this study are available from the corresponding author upon reasonable request.

Ethical Approval

All animal experiments were approved by the local ethics committee and performed according to the guidelines of the Canadian Council on Animal Care.

Animals

Twelve-week-old male wild-type (MK2$^{+/+}$) and MK2-deficient (MK2$^{-/-}$) littermate mice, on a mixed 129/Ola x C57BL/6J genetic background, were used. These mice have been described previously.[34] MK2$^{-/-}$ mice are viable, fertile, and show no behavioral or physiological defects.

In Vivo Cardiac Function
Radio Telemetry

Radio telemetry was used for continuous recordings of heart rate and ECG data in conscious unrestrained mice. MK2$^{+/+}$ mice and age-matched MK2$^{-/-}$ mice were instrumented, under isoflurane anesthesia (2.5% in O$_2$, 0.5 L/min for induction and 1.5% for maintenance), with OpenHeart single-channel telemetry transmitters (Data Sciences International, Arden Hills, MN) as described previously.[35] For analgesia, buprenorphine (0.05 mg/kg) was administered before and every 8 hours for 48 hours after surgery. Leads were placed in the conventional ECG lead II position with the positive transmitter lead located on the left anterior chest wall above the apex of the heart and the negative lead located on the right shoulder. Mice were provided with food and water ad libitum and maintained on a 12:12 hour day-night cycle. One week after surgery, data acquisition was initiated at a sampling frequency of 1 kHz and maintained for 48 hours. Recordings were analyzed with ECG Auto (version 2.8; EMKA Technologies, Paris, France). Briefly, the first 10 minutes of every 3-hour period was analyzed for the entire 48 hours of recording. A smoothing of 1 ms and notch filter of 60 Hz were used to reduce noise. Signals were averaged from 10 consecutive beats. ECG parameters were obtained through an automated signal detection using typical traces. The analyst was blinded as to genotype, and the mice shared the same library of typical traces. The QT interval was corrected for differences in R-R interval using the standard formula for mice (QTc=QT/(RR/100)$^{1/2}$).[36] Heart rate variability was analyzed using Kubios HRV Standard (Version 3.0.0; Kubios, Kuopio, Finland) to fit an ellipse to a Poincaré plot (R–R$_n$ versus R–R$_{n+1}$) of R-R interval data. Results were expressed as the ratio of the SD on the short axis (SD1) versus the SD on the long axis (SD2) of the ellipse. SD1 reflects short-term heart rate variability whereas SD2 reflects both short-term and long-term heart rate variability.[37]

Surface ECGs

Surface ECG recordings were assessed on male MK2$^{+/+}$ and MK2$^{-/-}$ mice, under anesthesia with 2% isoflurane (100% O$_2$, flow rate of 1 L/min), before and after intravenous injection of isoproterenol (0.1 µg/g) as previously described.[38]

Transthoracic Echocardiography

Transthoracic echocardiographic imaging was performed on mice, sedated with isoflurane (2% in 100% O$_2$, flow rate of 1 L/min), 1 day before constriction of the transverse aorta (TAC), for baseline evaluation, and 1 day before euthanasia. In the 8-week cohort, echocardiographic imaging was also performed 2 weeks after surgery. Examinations were carried out with a linear array i13L probe (10–14 MHz) using a

Vivid 7 Dimension ultrasound system (GE Healthcare, Horten, Norway). The operator was blinded to the genotype of the mice. All parameters and calculations related to left ventricular (LV) and right ventricular (RV) structure, LV and RV systolic function, LV and RV diastolic function, left atrium dimensions, and myocardial performance index were obtained as previously described.[39–41]

Millar Catheterization

Hemodynamic parameters were evaluated using a Mikro-Tip pressure transducer catheter (Millar Instruments, Houston, TX) in mice anesthetized with 2% isoflurane (100% O_2, flow rate of 1 L/min). Body temperature was monitored and maintained at 37°C using a heating pad. The catheter was inserted into the left ventricle through the carotid as previously reported.[40] Recordings were analyzed using IOX software version 2.5.1.6 (EMKA Technologies, Sterling, VA).

Transverse Aortic Constriction

TAC was performed in 12-week-old male mice sedated with isoflurane gas as previously described.[40] The surgeon was blinded as to the genotype of the mice. Sham animals underwent the identical surgical procedure, but the aorta was not constricted. Two or 8 weeks after surgery, mice were anesthetized with pentobarbital and euthanized, hearts removed, weighed, snap-frozen in liquid nitrogen-chilled 2-methyl butane, and stored at −80°C. Pentobarbital, rather than isoflurane, was always used before euthanaisa as isoflurane activates p38 MAP kinase in the mouse heart (data not shown).

Ex Vivo Cardiac Function
Ex Vivo Working Heart Perfused in Semirecirculating Mode

Hearts were isolated from fed mice and perfused under normoxic conditions for 30 minutes to evaluate basal function. To assess the impact of isoproterenol, hearts from a second group of mice were perfused under normoxic conditions for 20 minutes after which isoproterenol (10 nmol/L) was added to the buffer and perfusion continued for an additional 20 minutes. All perfusions were carried out at a fixed preload (15 mm Hg) and afterload (50 mm Hg, except following addition of isoproterenol [see below]), and using a semirecirculating modified Krebs-Henseleit buffer containing a mix of substrates and hormones as previously described[42] in the absence (11 mmol/L glucose, 1.5 mmol/L lactate, 0.2 mmol/L pyruvate, 50 mmol/L carnitine, 0.8 nmol/L insulin, and 5 nmol/L

epinephrine) or presence of palmitate (11 mmol/L glucose, 1.5 mmol/L lactate, 0.2 mmol/L pyruvate, and 0.7 mmol/L palmitate bound to 3% dialyzed albumin, 50 mmol/L carnitine, 0.8 nmol/L insulin, and 5 nmol/L epinephrine). During perfusion in the presence of isoproterenol (10 nmol/L) the afterload was increased to 60 mm Hg. Functional parameters were monitored throughout the perfusion (iox2 data acquisition software, EMKA Technologies): Data shown were acquired during the final 5 minutes of each perfusion.

In Vitro Analyses on Isolated Ventricular Myocytes or Mitochondria
Ca^{2+} Transients and Caffeine-Induced Ca^{2+} Transients

Ca^{2+} transients and sarcoplasmic reticulum Ca^{2+} content were assessed in cardiac ventricular myocytes isolated from 12-week-old male $MK2^{+/+}$ and $MK2^{-/-}$ mice as described previously.[43] Briefly, myocytes were incubated with 10 µmol/L Fluo-4 AM (Molecular Probes, Carlsbad, CA), then transferred to a perfusion chamber on the stage of a Zeiss LSM 510 microscope (Carl Zeiss AG, Jena, Germany), and perfused with a Tyrode solution. The perfusion chamber was fitted with bipolar platinum electrodes attached to a Grass SD9 stimulator and maintained at 37°C. To assess Ca^{2+} transients, myocytes were continuously field stimulated at a rate of 2 Hz. To assess the sarcoplasmic reticulum Ca^{2+} content, myocytes first received 10 conditioning pulses at 2 Hz to ensure that each cell had a similar activation history. Upon completion of the conditioning pulses, 10 µmol/L caffeine was applied to the myocyte for 10 seconds via a rapid solution switcher. Changes in free Ca^{2+} were measured in line scan mode with excitation at 488 nm and emission measured at 505 to 530 nm. Myocytes were scanned repeatedly along the length of the cell at 1.5-ms intervals for 7 seconds. Sequential scans were stacked to create a two-dimensional image. Image J (National Institutes of Health, Bethesda, MD) was used to visualize the Ca^{2+} transients, and the data were analyzed with pCLAMP 8.2 (Molecular Devices).

Isolation of Cardiac Mitochondria and Mitochondrial Respiration Measurements

Subsarcolemmal mitochondria were isolated from adult mouse hearts as described previously.[44] Subsarcolemmal mitochondria were resuspended in KME buffer (100 mmol/L KCl, 50 mmol/L MOPS, 0.5 mmol/L EGTA) at a final concentration of 25 mg mitochondrial protein/mL. To assess respiration, subsarcolemmal mitochondria were suspended (0.25 mg

Table 1.   Primers Used for Quantitative Polymerase Chain Reaction

Gene	Name	Genebank ID	Sense	Antisense
Acadm	Acyl-coenzyme A dehydrogenase, medium-chain	NM_0079382	GTGCGGTGTCCAACACAGA	TTCTACCGGCATCTTCTCCTC
Gapdh	Glyceraldehyde-3-phosphate dehydrogenase	NM_008084	CTGCACCACCAACTGCTTAGC	ACTGTGGTCATGAGCCCTTCCA
Lipe	Hormone-sensitive lipase	NM_010719	GGCACAGACCTCTAAATCCC	CCGCTCTCCAGTTGAACC
Myh7	β-myosin heavy chain	NM_001361607	AGGGTGGCAAAGTCACTGCT	CATCACCTGGTCCTCCTTCA
Nppa	Atrial natriuretic peptide	NM_008725	GTGCGGTGTCCAACACAGA	TTCTACCGGCATCTTCTCCTC
Pdk4	Pyruvate dehydrogenase kinase, isoenzyme-4	NM_013743	GTGATGTGGTAGCAGTAGTC	ATGTGGTGAAGGTGTGAAGG
Ppargc1a	Peroxisome proliferator-activated receptor γ coactivator 1-α	NM_008904	TGGATGAAGACGGATTGC	TGGTTCTGAGTGCTAAGAC
Ucp3	Uncoupling protein 3	NM_009464	TCCGATTTCAAGCCATGATACG	GTCACCATCTCAGCACAGTTG

protein in 0.5 mL) in a respiration buffer containing 100 mmol/L KCl, 50 mmol/L MOPS, 5 mmol/L KH_2PO_4, 1 mmol/L EGTA, and 0.1% fatty acid-free BSA, pH 7.0. Oxygen consumption was measured using a Clark-type electrode. After recording the basal respiration rate, the following substrate conditions were assessed: (1) 10 mmol/L glutamate plus 5 mmol/L malate, (2) 10 mmol/L pyruvate plus 5 mmol/L malate, (3) 10 mmol/L palmitoyl carnitine plus 5 mmol/L malate, and (4) 10 mmol/L succinate plus 7.5 µmol/L rotenone as previously described.[44] State 3 respiration was measured in the presence of 200 µmol/L ADP, and state 4 respiration was measured with the addition of oligomycin (4 µmol/L).

Assessing Ca²⁺-Induced Mitochondrial Permeability Transition Pore Opening

The calcium dependency for mitochondrial permeability transition pore (mPTP) opening in subsarcolemmal mitochondria was determined as previously described.[45] In short, mitochondria (0.5 mg) were resuspended in 2.0 mL of assay medium containing 100 mmol/L KCl, 50 mmol/L MOPS, 5 mmol/L KH_2PO_4, 5 µmol/L EGTA, 1 mmol/L $MgCl_2$, 5 mmol/L glutamate, and 5 mmol/L malate and assayed for Ca^{2+} uptake in a fluorescence spectrophotometer at 37°C. $CaCl_2$ (5 mmol/L) was infused at a rate of 2 µL/min and the concentration of extramitochondrial free Ca^{2+} was determined using 0.1 mmol/L Fura-6F by monitoring fluorescence emission at 550 nm with excitation wavelengths for the free and calcium-bound forms of 340 and 380 nm, respectively. The cumulative Ca^{2+} load that was required to induce mPTP opening was determined from a semilog plot of the extramitochondrial $[Ca^{2+}]$ versus the cumulative Ca^{2+} load and defined as the amount of infused Ca^{2+} required to induce a sharp increase in extramitochondrial $[Ca^{2+}]$.[46] Analyses were done by a single investigator who was blinded as to the identity of the samples.

Measuring Reactive Oxygen Species

To determine whether abolishing MK2 activity affected mitochondrial generation of reactive oxygen species, hydrogen peroxide production was measured in respiring mitochondria as previously described.[45] Briefly, 0.75 mg of mitochondria were incubated in respiration buffer containing malate and glutamate to which 5 U/mL horseradish peroxidase, 40 U/mL Cu-Zn superoxide dismutase, and 1 µmol/L Amplex Red were added. Superoxide generation was measured with sequential additions of ADP (0.5 mmol/L), oligomycin (1.25 µg/mL), and rotenone (1 µmol/L). H_2O_2 production was measured as an increase in fluorescence of Amplex Red. The experiment was terminated by the addition of 1 nmol H_2O_2 to calibrate the dye response.

Cardiac Tissue Analyses
Histologic Analysis

Hearts were embedded in Tissue-Tek O.C.T. compound (Sakura Finetek USA, Inc., Torrance, CA), and transverse cryosections (8 µm) of the ventricles were prepared and stained with Masson's trichrome. Two regions on each of 3 separate sections per heart were analyzed by a histology technician who was blinded to the identity of the mice. Images were taken at ×40 using an Olympus BX46 microscope (Olympus Corp., Shinjuku, Japan). Collagen content was quantified by color segmentation using Image Pro Plus version 7 (Media Cybernetics, Rockville, MD) and expressed as a percentage of the surface area. Perivascular collagen was excluded from the measurements. Myocyte diameter was determined in trichrome-stained cryosections using Image Pro Plus.
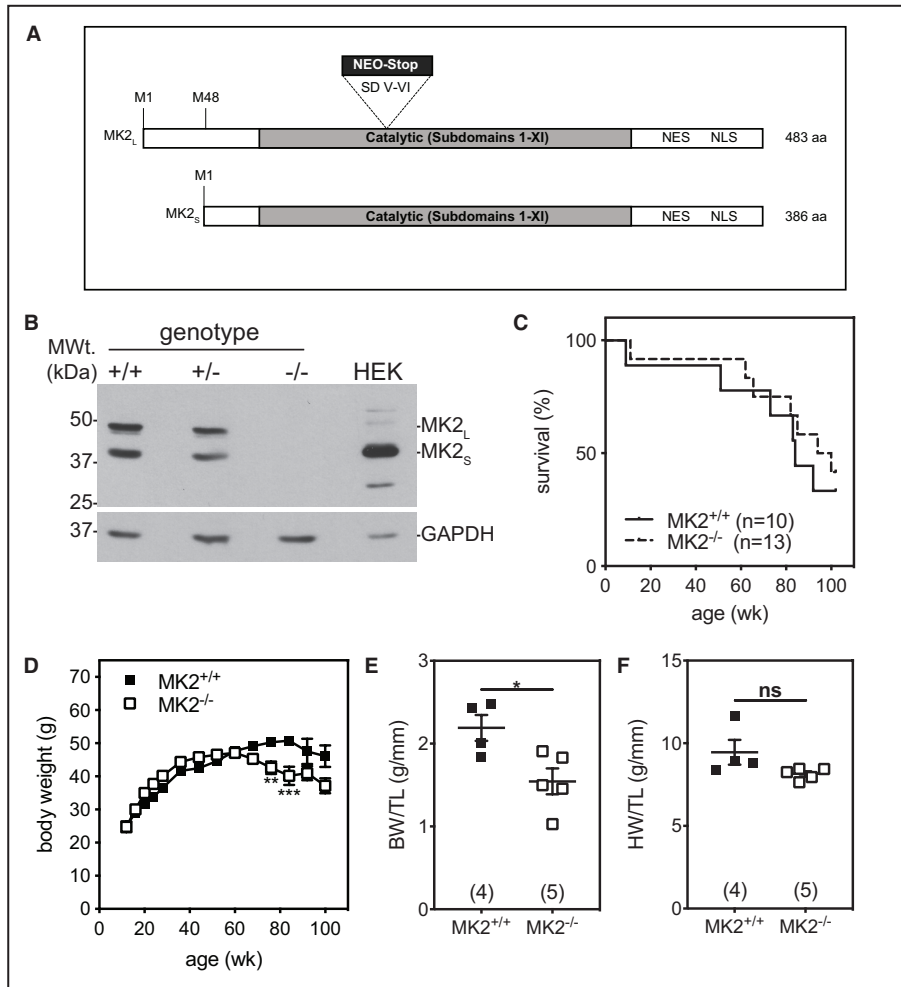
Figure 1. MK2 deficiency does not alter survival but enhances aging-dependent weight loss.
A, Scheme showing the long (MK2$_L$) and short (MK2$_S$) forms of MK2 resulting from the use of alternative translation initiation start sites along with the neomycin-resistance gene inserted into the exon encoding catalytic subdomains (SD) V and VI, resulting in an in-frame translation stop codon (NEO-Stop).[34,51] **B**, Representative image showing immunoreactive bands of long (MK2$_L$) and short (MK2$_S$) forms of MK2 in heart lysates from 12-week-old MK2$^{+/+}$, MK2$^{+/-}$, and MK2$^{-/-}$ mice. Numbers on left indicate molecular mass (in kDa). **C**, Kaplan-Meier survival curves for MK2$^{+/+}$ (n=10) and MK2$^{-/-}$ (n=13) mice up to age 102 weeks. Mantel-Cox tests indicated that the survival curves did not differ significantly (P=0.580). **D**, Changes in body weight in MK2$^{+/+}$ and MK2$^{-/-}$ mice up to 102 weeks of age. **E**, Body weight (BW) and (**F**) heart weight (HW), both normalized to tibia length (TL) in 102-week-old MK2$^{+/+}$ and MK2$^{-/-}$ mice. Data are expressed as mean±SEM. *P<0.05, **P<0.01, ***P<0.001. HEK indicates human embryonic kidney; M1, methionine-1; M48, methionine-48; MK2, mitogen-activated protein kinase–activated protein kinase-2; MWt, molecular weight; NES, nuclear export signal; NLS, nuclear localization sequence; and ns, not significant.

Quantitative Real-Time Polymerase Chain Reaction

Total cellular RNA was isolated from transverse cryosections (14 µm) of murine ventricular myocardium using RNeasy Micro kits (Qiagen Inc., Hilden, Germany) with minor modifications. Total RNA was extracted by vortexing tissue section in 300 µL TRIzol reagent (Sigma-Aldrich, St. Louis, MO) for 30 seconds. After incubating at ambient temperature for 5 minutes, 60 µL of chloroform was added, samples were again vortexed and maintained at ambient temperature for an additional 2 to 3 minutes. After centrifugation for 15 minutes at 18 300g and 4°C, the upper aqueous phase was collected, diluted with an equal volume of 70% ethanol, and total RNA purified on Qiagen columns according to the manufacturer's instructions. Finally, total RNA was eluted with 14 µL of distilled, RNAse-free water. cDNA synthesis was performed as described previously.[12]

Table 2.   Echocardiographic Parameters of LV Structure and Function in 12-Week-Old MK2$^{+/+}$ and MK2$^{-/-}$ Mice

	MK2$^{+/+}$	MK2$^{-/-}$
n	122	127
R-R interval, ms	176±3	199±4*
Heart rate, beats/min	341±20	304±17*
LV structure		
LVAW$_d$, mm	0.758±0.007	0.764±0.007
LVPW$_d$, mm	0.736±0.008	0.714±0.007†
LVD$_d$, mm	4.06±0.03	3.90±0.03‡
LVD$_s$, mm	2.61±0.03	2.56±0.04
LV mass, mg	111±2	102±2*
LV mass/LVD$_d$, mg/mm	27.2±0.3	26.1±0.3†
LV mass/BW, mg/g	3.71±0.05	3.62±0.05
LV systolic function		
LVFS, %	35.9±0.6	34.6±0.7
LVEF, %	71.5±0.7	69.6±0.9
LVV$_d$, µL	181±4 (78)	151±4 (77)*
LVV$_s$, µL	51.7±2.2 (79)	45.4±2.5 (77)
SV, µL	34.8±0.8 (76)	32.2±0.8† (76)
CO, mL/min	11.4±0.2 (76)	9.78±0.28* (76)
S$_L$, cm/s	2.23±0.04	1.98±0.04*
S$_S$, cm/s	2.38±0.04	2.14±0.04‡
LV diastolic function		
Transmitral flow		
E, cm/s	75.0±1.0	74.6±1.4
EDT, ms	35.2±0.8	38.7±0.8§
ED rate, m/s^2	22.8±0.6	20.6±0.6§
A, cm/s	47.7±0.7 (109)	48.8±0.7 (120)
E/A	1.62±0.02 (109)	1.59±0.05 (121)
Lateral E$_m$, cm/s	2.23±0.06 (110)	1.98±0.05 (121)§
Lateral A$_m$, cm/s	2.33±0.07 (112)	2.10±0.06 (121)§
Lateral E$_m$/A$_m$	1.01±0.04 (109)	1.01±0.03 (120)
Lateral E/E$_m$	36.7±1.0 (110)	40.0±1.1 (121)†
Septal E$_m$, cm/s	2.68±0.06 (112)	2.34±0.05 (120)*
Septal A$_m$, cm/s	2.55±0.06 (113)	2.27±0.06 (121)‡
Septal E$_m$/A$_m$	1.11±0.03 (112)	1.10±0.04 (118)
Septal E/E$_m$	29.3±0.6 (112)	32.7±0.7 (120)*
Pulmonary venous flow		
Upper S, cm/s	18.0±0.5 (100)	16.1±0.6 (97)§
Upper D, cm/s	39.6±0.7 (100)	32.9±0.8 (97)*
Upper S/D	0.463±0.011 (100)	0.507±0.022 (97)
Lower S, cm/s	47.6±1.0 (100)	43.9±1.1 (97)§
Lower D, cm/s	31.6±0.7 (100)	29.4±0.8 (97)†
Lower S/D	1.57±0.04 (100)	1.56±0.04 (97)
S slope, m/s^2	4.24±0.14 (100)	3.48±0.12 (97)*
S/D mean	1.01±0.02 (100)	1.03±0.02 (97)
LV isovolumetric relaxation time		
IVRT, ms	13.2±0.5	16.3±0.8‡

(Continued)

Table 2.   Continued

	MK2$^{+/+}$	MK2$^{-/-}$
IVRTc	0.98±0.03	1.14±0.05§
LA dimensions		
LAD$_s$, mm	2.24±0.03 (107)	2.12±0.04 (109)†
LAD$_d$, mm	1.72±0.03 (85)	1.65±0.04 (90)
LAFS, %	20.6±0.5 (85)	20.4±0.7 (90)
MPI		
Septal MPI, %	61.1±2.6 (121)	61.2±1.8
Lateral MPI, %	62.5±2.6 (121)	62.9±2.2
Global MPI, %	46.7±1.5 (121)	52.0±1.5 (126)§

Data are reported as mean±SEM. n=122 and 127 for MK2$^{+/+}$ and MK2$^{-/-}$, respectively, unless otherwise indicated by numbers in parentheses. A indicates transmitral flow late (atrial) filling velocity; A$_m$, mitral annulus peak velocity during atrial diastolic filing; CO, cardiac output; D, peak velocity during pulmonary venous diastolic flow; E, transmitral flow early filling velocity; ED, E wave deceleration; EDT, E wave deceleration time; E$_m$, mitral annulus peak velocity during early diastolic filing; IVRT, isovolumic relaxation time; IVRTc, heart rate-corrected IVRT; LAD$_d$, left atrium dimension at end cardiac diastole; LAD$_s$, left atrium dimension at end cardiac systole; LV, left ventricular; LVAW$_d$, left ventricular anterior wall thickness at end cardiac diastole; LVD$_d$, left ventricular dimension at end cardiac diastole; LVD$_s$, left ventricular dimension at end cardiac systole; LVEF, left ventricular ejection fraction; LVFS, left ventricular fractional shortening; LVPW$_d$, left ventricular posterior wall thickness at end cardiac diastole; LVV$_d$, left ventricular volume at end cardiac diastole; LVV$_s$, left ventricular volume at end cardiac systole; MK2, mitogen-activated protein kinase–activated protein kinase-2; MPI, myocardial performance index; S, peak velocity during pulmonary venous systolic flow; SD slope, pulmonary venous systolic flow decelerating slope; S$_L$, basal lateral systolic velocity; S$_S$, basal septal systolic velocity; and SV, stroke volume.

*$P<0.0001$ for MK2$^{-/-}$ vs MK2$^{+/+}$.
†$P<0.05$ for MK2$^{-/-}$ vs MK2$^{+/+}$.
‡$P<0.001$ for MK2$^{-/-}$ vs MK2$^{+/+}$.
§$P<0.01$ for MK2$^{-/-}$ vs MK2$^{+/+}$.

Quantitative polymerase chain reaction was performed by a single observer in a blinded manner. The following genes were selected: (1) key metabolic enzymes, namely, medium-chain acyl-CoA dehydrogenase (*Acadm*) and hormone-sensitive lipase (*Lipe*); (2) a transcriptional coactivator acting as a master regulator of mitochondrial function and regulating metabolic gene expression, namely, peroxisome proliferator-activated receptor γ coactivator 1-α (*Ppargc1a*); (3) mitochondrial uncoupling protein 3 (*Ucp3*), (4) a marker gene of the fetal phenotype, namely, myosin heavy-chain β (*Myh7*); and (5) a marker of early cardiac remodeling, namely, atrial natriuretic factor (*Nppa*). Primers used are listed in Table 1.[40,47] The abundance of mitochondrial calcium uptake 2 (*Micu2*) was performed by TaqMan assay (Assay ID: Mm00801666_g1, FAM-MGB) and normalized to *Gapdh* (Assay ID: Mm99999915_g1, VIC-MGB) as described previously.[48]

Biochemical Analyses

Activities of the mitochondrial marker enzymes citrate synthase, succinate dehydrogenase, isocitrate dehydrogenase, and medium-chain acyl–coenzyme A

Table 3. Echocardiographic Parameters of RV Structure and Function in 12-Week-Old MK2⁺/⁺ and MK2⁻/⁻ Mice

	MK2$^{+/+}$	MK2$^{-/-}$
n	78	77
RV structure		
RVAW$_d$, mm	0.316±0.006	0.299±0.007
RVD$_d$, mm	1.81±0.02	1.71±0.03*
RVAW$_d$/RVD$_d$	0.175±0.003	0.175±0.004
TAPSE, mm	1.26±0.02	1.21±0.01†
RV systolic function		
S$_R$, cm/s	3.32±0.07	2.81±0.07‡
RV diastolic function		
Transtricuspid flow		
E$_t$, cm/s	30.3±0.8 (77)	30.7±1.2
E$_t$DT, ms	29.3±1.3	29.4±1.3
E$_t$D rate, m/s²	10.2±0.4 (77)	10.2±0.5
A$_t$, cm/s	42.4±0.9 (68)	42.6±1.3 (66)
E$_t$/A$_t$	0.693±0.024	0.727±0.045
Lateral E$_m$, cm/s	3.34±0.10 (71)	2.72±0.08 (65)‡
Lateral A$_m$, cm/s	3.22±0.10 (71)	2.83±0.11 (65)*
Lateral E$_m$/A$_m$	1.09±0.04 (71)	1.08±0.07 (65)
Lateral E/E$_m$	9.09±0.30 (70)	10.5±0.4 (65)*
Pulmonary artery flow		
AT, ms	21.9±0.7 (75)	23.1±0.8 (76)
AT/RVET	26.7±0.7 (75)	24.9±0.7 (76)
RV MPI		
TV$_{CO}$, ms	102±2 (77)	115±2 (76)‡
RVET, ms	82.2±1.4 (75)	92.6±1.7‡
Lateral MPI, %	39.2±0.8	40.4±0.9
Global MPI, %	24.5±1.2 (74)	27.6±1.5 (73)

Data are reported as mean±SEM. n=78 and 77 for MK2$^{+/+}$ and MK2$^{-/-}$, respectively, unless otherwise indicated by numbers in parentheses. A$_m$, tricuspid annulus peak velocity during late (atrial) diastolic filing; AT, pulmonary arterial flow acceleration time; A$_t$, transtricuspid flow late (atrial) filling velocity; E$_m$, tricuspid annulus peak velocity during early diastolic filing; E$_t$, transtricuspid flow early filling velocity; EtD rate, transtricuspid early filling deceleration rate; E$_t$DT, transtricuspid early filling deceleration time; MK2, mitogen-activated protein kinase–activated protein kinase-2; MPI, myocardial performance index; RV, right ventricular; RVAW$_d$, right ventricular anterior wall thickness at end cardiac diastole; RVD$_d$, right ventricular diameter at end cardiac diastole; RVET, right ventricular ejection time; S$_R$, right ventricular lateral wall systolic velocity; TAPSE, tricuspid annulus plane systolic excursion; and TV$_{CO}$; tricuspid valve closure to opening time.

*$P<0.01$ for MK2$^{-/-}$ vs MK2$^{+/+}$.

†$P<0.05$ for MK2$^{-/-}$ vs MK2$^{+/+}$.

‡$P<0.0001$ for MK2$^{-/-}$ vs MK2$^{+/+}$.

dehydrogenase were measured spectrophotometrically in LV myocardium homogenates.[45,49]

Immunoblotting

SDS-PAGE and immunoblotting were performed as described previously[33] with a slight modification. Following electrophoretic transfer to 0.22 µm nitrocellulose, membranes were rinsed in PBS and fixed with glutaraldehyde[50] before blocking.

Statistical Analysis

Results are reported as the mean±SEM. The Shapiro-Wilks test for normality was performed on all data. Statistical differences between 2 groups were tested using either an unpaired, 2-tailed *t* test or a Mann-Whitney test (nonnormal data). For comparisons involving >2 groups, 1-way ANOVA followed by Bonferroni's (compare selected means) test was performed. For comparisons involving 2 independent variables, 2-way ANOVA followed by either Tukey's (compare all means) or Bonferroni's (compare selected means) tests were performed. Nonnormal data sets were log-transformed before ANOVA. Survival curves were compared using Mantel-Cox log-rank tests. Results were considered statistically significant when *P* values were <0.05. Statistical analyses were performed using Prism version 9.0 beta for Mac OS X (GraphPad Software, La Jolla, CA).

RESULTS

There are 2 known variants of MK2, long and short, which result from the use of alternative translation initiation start sites (Figure 1A and 1B).[51] The development and general phenotypic characterization of MK2$^{-/-}$ and MK2$^{+/+}$ mice have been described elsewhere,[34] and the abundance of MK2 immunoreactivity in lysates prepared from the ventricular myocardium correlated with genotype (Figure 1B). At 12 weeks of age, MK2-deficient mice had similar body weight (MK2$^{+/+}$: 29.7±0.4 g, n=141, MK2$^{-/-}$: 28.7±0.4 g, n=143; *P*=0.067); at 16 weeks of age, they were characterized by a slight reduction in rectal temperature (MK2$^{+/+}$: 33.1±0.4°C, n=10, MK2$^{-/-}$: 32.0±0.4°C, n=12; *P*<0.05).

MK2$^{-/-}$ Mice Show Slight Changes Both in LV and RV Function and Bradycardia When Assessed In Vivo
Echocardiographic Analyses

Echocardiographic imaging at 12 weeks of age revealed a prolonged R-R interval (MK2$^{+/+}$: 176±3 ms, n=122, MK2$^{-/-}$: 199±4 ms, n=127; *P*<0.0001) with modest differences in LV structure and function in MK2-deficient mice (Table 2). In MK2$^{-/-}$ mice, several parameters reflecting LV structure were reduced significantly, including a 3% decrease in LV end-diastolic posterior wall thickness (MK2$^{+/+}$: 0.736±0.008 mm, n=122, MK2$^{-/-}$: 0.714±0.007 mm, n=127; *P*<0.05), a 4% decrease in LV end-diastolic diameter (MK2$^{+/+}$: 4.06±0.03 mm, n=122, MK2$^{-/-}$: 3.90±0.03 mm, n=127; *P*<0.001) and an 8% decrease in LV mass (MK2$^{+/+}$: 111±2 mg, n=122, MK2$^{-/-}$: 102±2 mg, n=127; *P*<0.0001). LV ejection fraction was not

Table 4. MK2 Deficiency Does Not Result in a Progressive Decline in Cardiac Function

	<6 mo		6–12 mo		12–18 mo		18–24 mo	
	MK2$^{+/+}$	MK2$^{-/-}$	MK2$^{+/+}$	MK2$^{-/-}$	MK2$^{+/+}$	MK2$^{-/-}$	MK2$^{+/+}$	MK2$^{-/-}$
n	10	13	10	12	9	12	6	9
R–R interval, ms	156±6	184±8*	148±3	178±5*	166±5	187±4	158±13	176±9
LV structure								
LVAW$_d$, mm	0.716±0.026	0.727±0.016	0.834±0.017	0.850±0.017	1.07±0.04	0.943±0.031*	1.10±0.04	1.00±0.03†
LVPW$_d$, mm	0.718±0.026	0.724±0.018	0.803±0.016	0.800±0.021	0.873±0.040	0.869±0.080	0.923±0.034	0.902±0.023
LVD$_d$, mm	3.98±0.05	3.84±0.12	4.20±0.04	4.27±0.06	4.34±0.09	4.56±0.06	4.32±0.10	4.33±0.12
LV mass, mg	102±6	98.2±6.4	132±3	139±5	175±7	175±11	184±6	171±8
LV mass/LVD$_d$, mg/mm	25.6±1.2	25.2±1.0	31.4±0.7	32.3±0.9	40.6±1.8	38.4±2.4	42.7±1.7	39.4±0.9
LV systolic function								
LVFS, %	38.1±1.2	35.3±1.8	39.9±0.5	36.2±1.2	36.6±1.3	33.5±2.2	37.4±1.0	34.6±1.2
LVEF, %	74.3±1.4	69.5±2.3	76.4±0.5	71.5±1.6	72.3±1.7	67.6±2.7	73.9±1.3	70.1±1.7
S$_L$, cm/s	2.58±0.11	2.33±0.10	2.86±0.08	2.44±0.09	1.76±0.09	1.71±0.06	1.82±0.10	1.67±0.12
S$_S$, cm/s	2.28±0.11	2.08±0.08	2.74±0.10	2.36±0.08‡	1.97±0.08	1.75±0.07	1.97±0.08	1.72±0.11
LV diastolic function								
Transmitral flow								
E, cm/s	60.4±1.9	53.2±3.9	68.1±1.4	62.4±1.5	73.7±3.3	70.4±2.9	79.2±5.7	73.2±2.6
EDT, ms	34.3±1.2	40.4±2.2	34.0±1.5	40.7±1.4‡	39.7±1.3	42.5±1.9	33.4±3.7	38.8±2.8
ED rate, m/s²	19.7±1.2	14.3±1.3‡	20.9±0.7	16.0±0.8*	19.2±1.3	17.1±0.7	25.6±2.9	20.1±12‡
A, cm/s	44.3±2.1	49.0±2.4	47.4±1.9	51.9±1.8	42.1±4.0	50.0±4.0	39.2±4.0	52.1±4.2
E/A	1.31±0.04	1.06±0.07	1.40±0.06	1.20±0.05	1.97±0.30	1.68±0.32	2.23±0.29	1.44±0.16‡
Lateral E$_m$, cm/s	2.43±0.12	1.75±0.12*	2.52±0.14	1.98±0.15‡	1.77±0.12	1.87±0.19	1.67±0.13	1.78±0.20†
Lateral E$_m$/A$_m$	0.796±0.065	0.723±0.050	0.818±0.044	0.664±0.061	0.938±0.057	0.97±0.11	0.813±0.034	0.99±0.13
Lateral E/E$_m$	26.3±1.7	25.7±1.8	28.6±1.8	36.1±2.0	46.2±4.5	41.7±4.9	46.8±1.3	43.5±5.2
Septal E$_m$, cm/s	2.30±0.24	1.95±0.15	2.53±0.17	2.11±0.19	2.44±0.19	2.1±0.13	2.22±0.30	2.27±0.26
Septal E$_m$/A$_m$	0.858±0.097	0.819±0.108	0.944±0.083	0.782±0.087	1.34±0.14	1.27±0.12	1.16±0.12	1.16±0.07
Septal E/E$_m$	30.2±2.9	28.1±2.2	29.0±2.1	34.1±2.6	33.4±2.4	36.4±2.9	36.8±3.0	34.7±4.7
Pulmonary venous flow								
S/D mean	1.28±0.10	1.22±0.09	1.19±0.09	1.40±0.06	1.33±0.13	1.65±0.16	1.22±0.14	1.60±0.12
LV isovolumetric relaxation time								
IVRTc	1.34±0.05	1.36±0.07	1.22±0.06	1.43±0.06	1.11±0.06	1.36±0.05‡	0.94±0.05	1.19±0.11
LA dimensions								
LAD$_s$, mm	2.06±0.10	1.67±0.06§	2.37±0.06	2.40±0.06	2.85±0.15	3.00±0.08	3.08±0.11	3.16±0.10†

(Continued)

Table 4. Continued

	<6 mo		6–12 mo		12–18 mo		18–24 mo	
	MK2+/+	MK2−/−	MK2+/+	MK2−/−	MK2+/+	MK2−/−	MK2+/+	MK2−/−
LAD$_d$, mm	1.68±0.10	1.31±0.07§	1.92±0.05	1.94±0.06	2.33±0.16	2.45±0.09	2.64±0.12	2.63±0.12†
LAFS, %	18.9±1.1	22.6±1.4	19.3±0.8	19.2±1.1	19.0±1.5	18.9±1.3	14.2±1.2	17.3±1.7
MPI								
Septal MPI, %	72.1±5.0	67.7±3.4	69.5±4.7	71.1±2.6	44.0±4.1	48.3±3.2	60.9±7.4	48.4±4.4
Lateral MPI, %	69.9±5.3	64.0±2.5	69.5±5.1	73.6±4.4	42.2±4.1	57.4±4.4	59.3±7.0	51.9±4.3
Global MPI, %	41.0±3.3	57.2±2.9‡	33.0±3.2	49.2±3.9*	25.2±2.8	42.6±2.6§	37.9±6.6	47.3±4.7

Data reported as mean±SEM. A indicates transmitral flow late (atrial) filling velocity; A$_m$, mitral annulus peak velocity during atrial diastolic filling; CO, cardiac output; D, peak velocity during pulmonary venous diastolic flow; E, transmitral flow early filling velocity; ED, E wave deceleration; EDT, E wave deceleration time; E$_m$, mitral annulus peak velocity during early diastolic filling; FS, fractional shortening; IVRT, isovolumic relaxation time; IVRTc, heart rate-corrected IVRT; LAD$_d$, left atrium dimension at end cardiac diastole; LAF$_s$, left atrium dimension at end cardiac systole; LVAW$_d$, left ventricular anterior wall thickness at end cardiac diastole; LVD$_d$, LV dimension at end cardiac diastole; LVD$_s$, LV dimension at end cardiac systole; LVEF, LV ejection fraction; LVPW$_d$, LV posterior wall thickness at end cardiac diastole; LVV$_d$, left ventricular volume at end cardiac diastole; LVV$_s$, left ventricular volume at end cardiac systole; MK2, mitogen–activated protein kinase–activated protein kinase-2; MPI, myocardial performance index; S, peak velocity during pulmonary venous systolic flow; SD slope, pulmonary venous systolic flow decelerating slope; S$_L$, basal lateral systolic velocity; S$_S$, basal septal systolic velocity; and SV, stroke volume.

*P<0.01 for MK2−/− vs MK2+/+.

†P<0.05 for an interaction between the effects of genotype and age.

‡P<0.05 for MK2−/− vs MK2+/+.

§P<0.001 for MK2−/− vs MK2+/+.

∥P<0.0001 for MK2−/− vs MK2+/+.

significantly different in MK2+/+ (71.5±0.7%; n=122) versus MK2−/− (69.6±0.9%, n=127) mice. Consistent with a reduced LV end-diastolic diameter and increased cardiac cycle length, cardiac output was reduced by 14% (MK2+/+: 11.4±0.2 mL/min, n=76, MK2−/−: 9.78±0.28 mL/min, n=76; P<0.0001) and both septal (MK2+/+: 2.38±0.04 cm/s, n=122, MK2−/−: 2.14±0.04 cm/s, n=127; P<0.001) and lateral (MK2+/+: 2.23±0.04 cm/s, n=122, MK2−/−: 1.98±0.04 cm/s, n=127; P<0.0001) wall systolic tissue velocities were decreased. Assessment of diastolic function revealed that the LV isovolumetric relaxation time, corrected for the differences in R-R interval, was prolonged by 16% in MK2−/− mice (rate-corrected isovolumetric relaxation time; MK2+/+: 0.98±0.03, n=122 MK2−/−: 1.14±0.05, n=127; P<0.01). There were no differences in the flow velocity of either early (E wave; MK2+/+: 75.0±1.0 cm/s, n=122; MK2−/−: 74.6±1.4 cm/s, n=127) or late (A wave; MK2+/+: 47.7±0.7 cm/s, n=109; MK2−/−: 48.8±0.7 cm/s, n=120) LV filling. In addition, E wave deceleration time was prolonged by 9.9% (MK2+/+: 35.2±0.8 ms, n=122; MK2−/−: 38.7±0.8 ms, n=127; P<0.01) and deceleration rate reduced by 9.6% (MK2+/+: 22.8±0.6 m/s^2, n=122; MK2−/−: 20.6±0.6 m/s^2, n=127; P<0.01) in MK2−/− hearts. Both septal and LV lateral mitral annular motion velocities (E$_m$, A$_m$) were reduced in MK2-deficient hearts, resulting in an increase in the ratio of transmitral early filling velocity to both lateral (MK2+/+: 36.7±1.0, n=110; MK2−/−: 40.0±1.1, n=121; P<0.05) and septal (MK2+/+: 29.3±0.6, n=112; MK2−/−: 32.7±0.7, n=120; P<0.0001) early diastolic mitral annular velocities, suggesting reduced LV compliance. Impaired LV compliance increases left atrial (LA) afterload and could result in LA enlargement. MK2−/− mice actually showed a slight decrease in LA diameter during systole (MK2+/+: 2.24±0.03 mm, n=107; MK2−/−: 2.12±0.04 mm, n=109; P<0.05) with no changes in LA fractional shortening. In addition, whereas a decrease in the ratio of the velocities of the systolic and diastolic waves of pulmonary venous flow would indicate impaired diastolic function, and this parameter is unaffected by increased R-R interval, the mean, upper, and lower pulmonary vein systolic/diastolic ratios did not differ between MK2+/+ and MK2−/− mice. In summary, MK2-deficiency did not alter LV systolic function but resulted in subtle signs of early diastolic dysfunction.

RV structure and function were also assessed by echocardiographic imaging (Table 3). There were no major differences in terms of RV structure other than a small reduction in RV end-diastolic diameter (MK2+/+: 1.81±0.02 mm, n=78; MK2−/−: 1.71±0.03 mm, n=77; P<0.01). Tricuspid annular plane systolic excursion, which correlates closely with the RV ejection fraction,[52] was slightly reduced (MK2+/+: 1.26±0.02 mm, n=78; MK2−/−: 1.21±0.01 mm, n=77; P<0.05) in
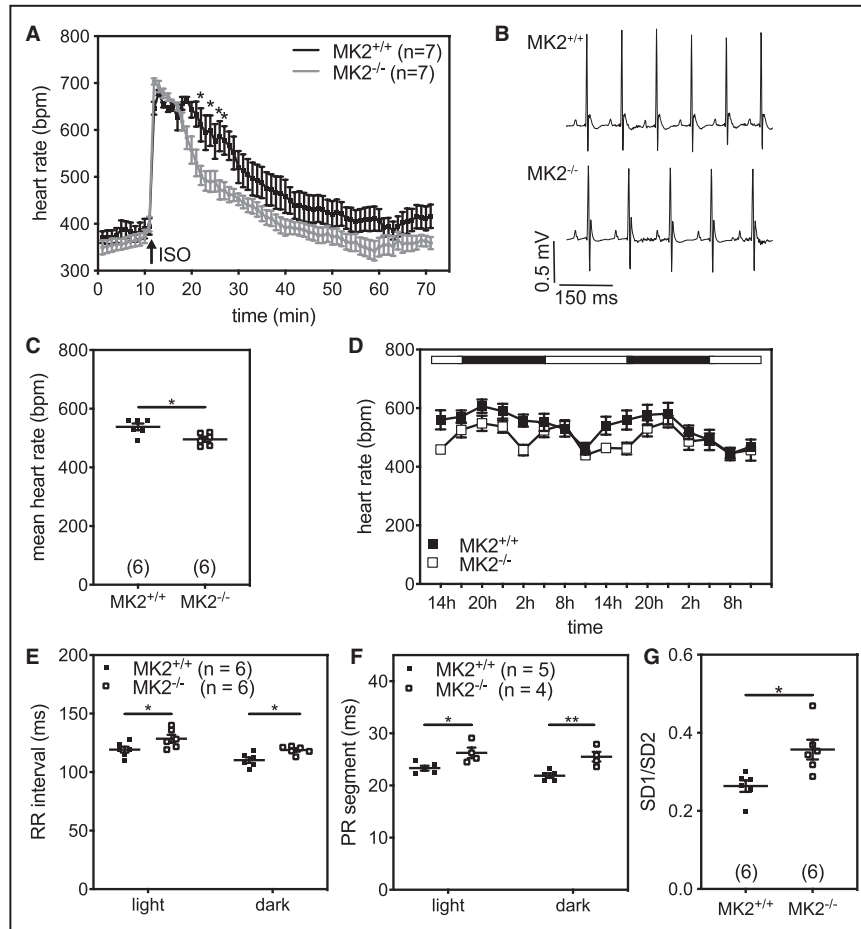
Figure 2. MK2$^{-/-}$ mice exhibited a slower heart rate in vivo.
A, In vivo heart rate assessment by surface electrocardiography in MK2$^{+/+}$ (n=7) and MK2$^{-/-}$ (n=7) mice anesthetized with isoflurane. Arrow indicates injection of isoproterenol (ISO; 0.1 mg/kg). *$P<0.05$ MK2$^{+/+}$ vs MK2$^{-/-}$, repeated-measures 2-way ANOVA with Bonferroni posttest. **B**, Representative ECGs obtained by radio telemetry in conscious unrestrained 12-week-old male MK2$^{+/+}$ (upper) and MK2$^{-/-}$ (lower) mice. **C**, Mean heart rates obtained from ECGs recorded over a 48-hour time period by radio telemetry in conscious unrestrained MK2$^{+/+}$ (n=6) and MK2$^{-/-}$ (n=6) mice. Data were extracted and analyzed in 3 hour intervals and then averaged separately for each mouse before calculating the mean heart rate for each group. **D**, Heart rates obtained from ECGs recorded over a 48-hour time period by radio telemetry in conscious unrestrained MK2$^{+/+}$ (n=6) and MK2$^{-/-}$ (n=6) mice. Data were extracted and analyzed in 3 hour intervals. Mice were maintained on a 12:12 hour light:dark cycle (18h00:6h00) with the bar at the top of the graph indicating light and dark cycles. The circadian rhythm is clearly visible. **E**, R-R interval and (**F**) P-R segment duration obtained from ECGs recorded over a 48-hour time period by radio telemetry in conscious unrestrained MK2$^{+/+}$ and MK2$^{-/-}$ mice. Data were extracted and analyzed in 3-hour intervals and then values for light and dark cycles averaged separately for each mouse before calculating the mean heart rate for each group. **G**, Mean 48 hour SD1/SD2 ratios for MK2$^{+/+}$ (n=6) and MK2$^{-/-}$ (n=6) mice where SD1 represents the standard deviation on the short axis and SD2 represents the standard deviation on the long axis of an ellipse fit to a plot of R-R$_n$ vs R-R$_{n+1}$. Data are expressed as mean±SEM. *$P<0.05$, **$P<0.01$. MK2 indicates mitogen-activated protein kinase–activated protein kinase-2.

MK2$^{-/-}$ mice as was the RV systolic tricuspid annular velocity (MK2$^{+/+}$: 3.32±0.07 cm/s, n=78; MK2$^{-/-}$: 2.81±0.07 cm/s, n=77; $P<0.0001$). In terms of RV diastolic function, peak velocities of early (E$_t$) and late (A$_t$) RV filling, in addition to the early RV filling wave deceleration time and deceleration rate, were similar in MK2$^{+/+}$ and MK2$^{-/-}$ hearts. Both early (E$_m$; MK2$^{+/+}$: 3.34±0.10 cm/s, n=71; MK2$^{-/-}$: 2.72±0.08 cm/s, n=65; $P<0.0001$) and late (A$_m$; MK2$^{+/+}$: 3.22±0.10 cm/s, n=71; MK2$^{-/-}$: 2.83±0.11 cm/s, n=72, $P<0.01$) diastolic lateral

Table 5. ECG Parameters Obtained From Conscious 12-Week-Old MK2$^{+/+}$ and MK2$^{-/-}$ Mice

	MK2$^{+/+}$	MK2$^{-/-}$
n	6	6
R-R interval, ms	115±3	123±2*
Heart rate, bpm	538±11	496±8*
P-R interval, ms	31.3±0.5 (5)	35.2±0.9 (4)†
P wave duration, ms	8.70±0.22 (5)	9.25±0.42 (4)
P-R segment, ms	22.6±0.4 (5)	25.9±1.0* (4)
QRS duration, ms	8.90±0.48	8.67±0.49
P wave amplitude, μV	13.2±2.7 (5)	12.7±2.2 (4)
QT interval, ms	46.1±0.6	49.1±1.1*
QTc	43.4±0.4	44.1±1.1

Data are reported as mean±SEM. n=6 unless otherwise indicated by numbers in parentheses. MK2 indicates mitogen-activated protein kinase–activated protein kinase-2.

*$P<0.05$.

$^†P<0.01$.

tricuspid annular motion velocities were reduced in MK2-deficient hearts, resulting in a 16% increase in the ratio of trans-tricuspid early filling velocity to early diastolic tricuspid annular velocity (E/E$_m$; MK2$^{+/+}$: 9.09±0.30, n=70; MK2$^{-/-}$: 10.5±0.4, n=65; $P<0.01$). Hence, echocardiographic assessment revealed that the deletion of MK2 resulted in changes in RV function similar to those observed in the LV.

We then examined the possible effect(s) of an MK2-deficiency on cardiac aging. Mantel-Cox tests indicated that the survival curves for wild-type (10) and MK2-deficient (13) male littermates did not differ significantly when assessed up to 102 weeks of age (Figure 1C, $P=0.580$). Although both MK2$^{+/+}$ and MK2$^{-/-}$ mice initially appeared to age similarly, body weight in MK2$^{-/-}$ mice peaked at 60 weeks of age and then began to decrease, whereas that of wild-type mice peaked at around 80 weeks of age (Figure 1D). At 102 weeks of age, the body weight of surviving MK2$^{-/-}$ mice was 29% lower than that of surviving MK2$^{+/+}$ mice (MK2$^{+/+}$: 2.29±0.16 g/mm, n=4; MK2$^{-/-}$: 1.55±0.16 g/mm, n=5; $P<0.05$) when normalized to tibia length (Figure 1E). At 102 weeks of age, surviving MK2$^{-/-}$ mice also showed a 14% decrease (MK2$^{+/+}$: 9.46±0.75 mg/mm, n=4; MK2$^{-/-}$: 8.15±0.16 mg/mm, n=5) in heart weight normalized to tibia length (Figure 1F), which did not reach significance. Food and water consumption of 88-week-old MK2-deficient mice did not differ significantly from that of wild-type littermates (data not shown). Cardiac structure and function were assessed in MK2$^{+/+}$ and MK2$^{-/-}$ mice by echocardiography every 4 (weeks 12–28) or 8 (weeks 28–100) weeks until 102 weeks of age. Data for each parameter were then binned into 4 age ranges (<6, 6–12, 12–18, 18–24 months) for each mouse and the mean and SEM determined for MK2$^{+/+}$ and MK2$^{-/-}$ mice (Table 4). MK2$^{-/-}$ mice displayed a

prolonged R-R interval throughout the study; however, in the second year of life, the difference no longer reached significance. Throughout the duration of the study, LV ejection fraction and fractional shortening in MK2-deficient mice did not differ significantly from that of wild-type littermates, indicating that systolic function was unaffected. When examined at 3 months of age, MK2-deficient mice showed signs of reduced compliance, suggesting early diastolic dysfunction (Table 2); however, this condition did not progress with age (Table 4). Specifically, peak E and A wave velocities, as well as regional E/E$_m$ ratios, did not differ significantly. E wave deceleration times were prolonged and the deceleration rate tended to be significantly slower in MK2$^{-/-}$ mice. Furthermore, in MK2-deficient mice, aging was not associated with LA dilation or changes in the pulmonary venous flow systolic/diastolic ratio, which are hallmarks of diastolic dysfunction. However, although the left atria were significantly smaller in MK2$^{-/-}$ mice, this difference was lost with age, suggesting that there may have been some degree of atrial remodeling in these mice over time. In summary, the absence of MK2 was associated with weight loss but no age-related progressive deterioration in systolic or diastolic function.

Heart Rate and Electrocardiography in Conscious Mice

As mentioned above, echocardiographic imaging, obtained under isoflurane anesthesia, revealed the R-R interval was prolonged in MK2$^{-/-}$ mice (Table 2), indicating a lower heart rate in these mice (MK2$^{+/+}$: 341±20 beats/min, n=122; and MK2$^{-/-}$: 306±17 beats/min, n=127; $P<0.0001$). Analysis by surface ECG revealed that when mice under isoflurane anesthesia were challenged with a single dose of isoproterenol (0.1 mg/kg), the heart rate of MK2$^{-/-}$ mice and MK2$^{+/+}$ mice increased to similar levels, whereas heart rate declined more rapidly in MK2$^{-/-}$ mice (Figure 2A). However, isoflurane lowers heart rate[53] and could, possibly, affect MK2$^{+/+}$ and MK2$^{-/-}$ mice differently. Hence, we next evaluated cardiac electrical activity in conscious unrestrained mice by radio telemetry over a period of 48 hours. Overall, the mean R-R interval in MK2$^{-/-}$ mice was 7% longer in comparison to their littermate MK2$^{+/+}$ mice even in the absence of anesthetic (MK2$^{+/+}$: 115±3 ms, n=6; MK2$^{-/-}$: 123±2 ms, n=6; $P<0.05$) (Table 5). Stated otherwise, the heart rate in MK2$^{+/+}$ mice was 538±11 bpm (n=6), whereas that of MK2$^{-/-}$ mice was 496±8 bpm (n=6; $P<0.05$) (Table 5, Figure 2C). In addition, the duration of the P-R segment was longer in MK2$^{-/-}$ mice (MK2$^{+/+}$: 22.6±0.4 ms, n=5; MK2$^{-/-}$: 25.9±1.0 ms, n=4; $P<0.05$) whereas the P wave duration, QRS duration, and QTc were unaffected (Table 5). An
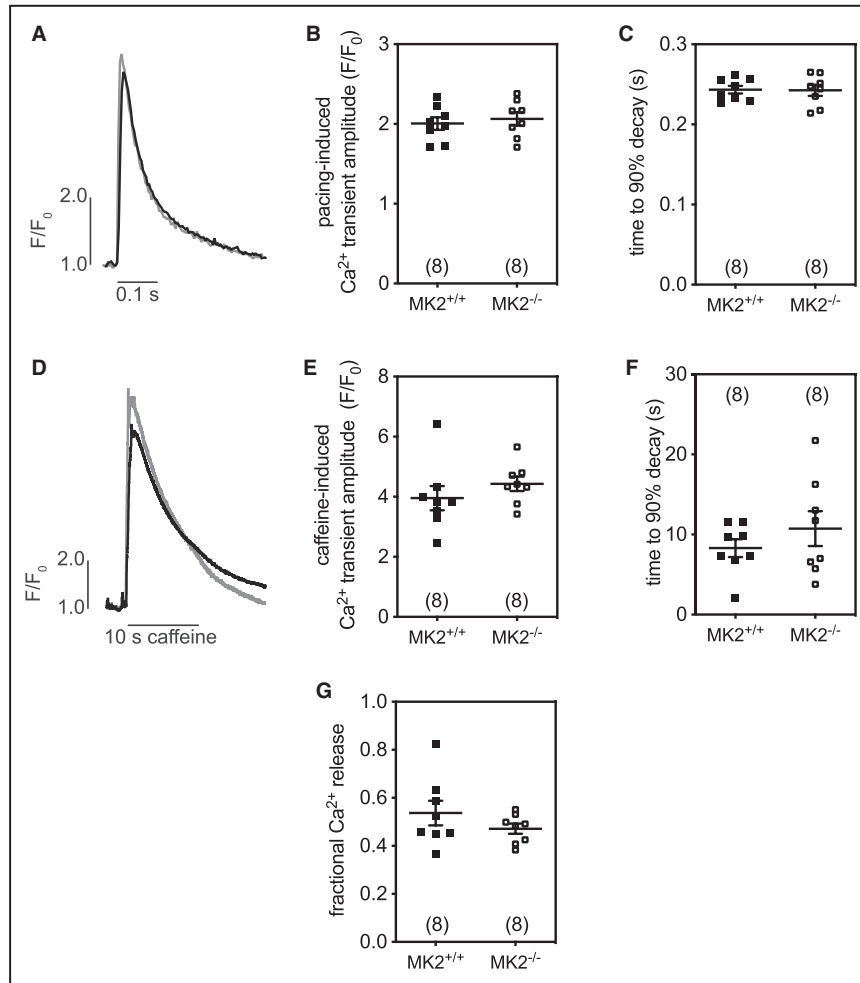
Figure 3. MK2 deficiency does not alter calcium transients or sarcoplasmic reticulum (SR) calcium content in adult cardiac ventricular myocytes.
Representative pacing-induced (**A**) and caffeine-induced (**D**) Ca^{2+} transients in ventricular myocytes isolated from 12-week-old $MK2^{+/+}$ (black) and $MK2^{-/-}$ (grey) mice, respectively. Mean Ca^{2+} transient amplitudes evoked by pacing (**B**) and caffeine (**E**) in $MK2^{+/+}$ and $MK2^{-/-}$ ventricular myocytes. **C** and **F**, Time to 90% decay for pacing- or caffeine-induced transients, respectively. **G**, Mean values for fractional SR calcium release (pacing-induced transient divided by caffeine-induced transient) in $MK2^{+/+}$ and $MK2^{-/-}$ ventricular myocytes. Data shown are mean±SEM from a total of 8 myocytes from 4 separate cell preparations. MK2 indicates mitogen-activated protein kinase–activated protein kinase-2.

examination of the circadian rhythm pattern of heart rate revealed MK2-deficient mice showed prolonged R-R intervals (Figure 2D and 2E) and P-R segments (Figure 2F) during both light and dark cycles. We next performed a nonlinear analysis of heart rate variability by plotting the R-R interval in the form of Poincaré plots ($R–R_n$ versus $R–R_{n+1}$), fitting the data to an ellipse, and determining the SD on the short (SD1) and long (SD2) axes of the ellipse. SD1 reflects short-term variability in heart rate, whereas SD2 reflects both short-term and long-term variability.[37] The SD1/SD2 ratio was significantly greater in MK2-deficient mice (Figure 2G). Both prolonged P-R segment, reflecting atrioventricular nodal conduction times, and

increased short-term variability in heart rate suggest autonomic regulation of heart rate is altered in MK2-deficient mice.

Calcium Transients Are Similar in Isolated Ventricular Cardiomyocytes From $MK2^{+/+}$ and $MK2^{-/-}$ Mice

In light of the differences in R-R interval and diastolic function observed in $MK2^{-/-}$ mice (Table 2, Table 4, Figure 2), we examined the effect of an MK2-deficiency on the amplitude and decay of Ca^{2+} transients evoked by field stimulation (2 Hz; Figure 3A through 3C) or superfusion with caffeine (10 seconds,

Table 6. Functional Parameters of Isolated Working MK2$^{+/+}$ and MK2$^{-/-}$ Mouse Hearts

Parameter	Control		+Isoproterenol		+Palmitate	
	MK2$^{+/+}$	MK2$^{-/-}$	MK2$^{+/+}$	MK2$^{-/-}$	MK2$^{+/+}$	MK2$^{-/-}$
n	8	10	7	10	11	11
Heart rate, beats/min	463±27	491±19	590±18*	575±12†	352±14*	323±14‡
Stroke volume, µL	26.8±3.6	24.2±2.0	22.3±2.4	20.4±1.6	31.5±1.3	31.3±1.8
Systolic ejection period, ms	28.8±3.6	31.1±2.4	24.1±2.5	25.9±1.0	40.1±2.1§	41.5±2.6
Diastolic filling period, ms	64.7±8.8	44.5±3.3	33.0±3.1‖	40.6±1.0¶	83.6±7.0	97.3±12.1‡
LVSP, mm Hg	113±5	122±5	122±5	137±6	103±3	103±2†
LVEDP, mm Hg	5.63±4.37	8.00±2.5	3.00±2.80	1.80±6.14	7.09±0.89	9.00±0.92
P$_{min}$, mm Hg	−7.75±1.99	−18.7±1.9§	−13.3±2.2	−27.1±3.5#	−5.73±1.68	−5.45±1.45**,††
Developed pressure, mm Hg	121±6	141±7	135±6	164±8††	110±5	108±2††,§§
+dP/dt, mm Hg/s	6096±612	5822±488	7112±730	6780±551	5245±176	5029±173
−dP/dt, mm Hg/s	4609±198	5357±215	5978±451	7347±523**	3860±159	3424±152**,††
Contraction time, ms	24.3±2.7	27.5±3.3	27.4±4.3	25.8±3.6	32.3±2.4	30.0±3.7
Relaxation time, ms	22.4±3.0	19.9±1.9	17.4±1.7	19.7±1.4	17.3±2.4	19.7±2.8
Contractility index, 1/s	103±8	89.9±5.5	103±10	89.8±8.1	94.8±3.6	95.9±4.2
Tau W, ms	8.6±1.4	6.5±0.8	6.7±0.6	5.7±0.8	6.5±1.2	8.0±1.5
Coronary flow, mL/min	3.63±0.59	4.05±0.42	4.35±0.39	4.91±0.36	2.96±0.54	2.46±0.25
Aortic flow, mL/min	8.34±1.35	7.60±0.53	8.84±1.64	6.80±0.88	8.02±0.60	7.58±0.32
Rate pressure product, mm Hg×beats/min×10^{-3}	55.6±4.1	68.9±3.0	80.3±5.2‖	94.1±4.9‖	38.4±2.0*	35.5±2.2‡,††
Cardiac output, mL/min	12.0±1.3	11.6±0.6	13.2±1.5	11.7±0.9	11.0±0.4	10.0±0.3
Cardiac power, mW	3.30±0.46	3.69±0.29	4.05±0.53	4.27±0.42	2.68±0.16	2.40±0.10
MVO$_2$, µmol/min	1.45±0.19	1.77±0.18	2.24±0.31	2.26±0.17	1.19±0.23	0.87±0.10†
Cardiac efficiency, mW×min/µmol	2.66±0.40	2.23±0.31	2.23±0.26	2.10±0.39	3.29±0.85	2.88±0.24
LDH release	13.7±3.0	13.4±3.9	15.5±3.7	16.2±3.5	12.4±2.8	12.8±1.7

Data reported as mean±SEM. HR indicates heart rate; LDH, lactate dehydrogenase; LVEDP, left ventricular end diastolic pressure; LVSP, left ventricular systolic pressure; MK2, mitogen-activated protein kinase–activated protein kinase-2; MVO$_2$, oxygen consumption; and P$_{min}$, minimum diastolic pressure.

*$P<0.001$ vs control-MK2$^{+/+}$.

†$P<0.05$ vs control-MK2$^{-/-}$.

‡$P<0.0001$ vs control-MK2$^{-/-}$.

§$P<0.05$ vs control-MK2$^{+/+}$.

‖$P<0.01$ vs control-MK2$^{+/+}$.

¶Indicates a significant interaction between the effects of isoproterenol and genotype; $P<0.05$.

#$P<0.0001$ vs iso-MK2$^{+/+}$.

**$P<0.001$ vs control-MK2$^{-/-}$.

††Indicates a significant interaction between the effects of substrate for energy production (carbohydrate±fatty acid) and genotype; $P<0.05$.

‡‡$P<0.05$ vs iso-MK2$^{+/+}$.

§§$P<0.01$ vs control-MK2$^{-/-}$.

10 µmol/L; Figure 3D through 3G) in isolated adult cardiac ventricular myocytes. Representative transients from MK2$^{+/+}$ and MK2$^{-/-}$ myocytes are respectively shown in Figure 3A and 3D. The mean data show in both conditions that neither the amplitude of the cytosolic Ca^{2+} transient nor the time to 90% transient decay for Ca^{2+}-transients differed significantly in cardiomyocytes from MK2$^{+/+}$ and MK2$^{-/-}$ mice after field stimulation (Figure 3B and 3C) or following caffeine superfusion (Figure 3E and 3F). In addition, the fractional release of Ca^{2+}, calculated by dividing the amplitude of the depolarization-induced Ca^{2+} transient by that of the caffeine-induced transient, was also similar in MK2$^{+/+}$ and MK2$^{-/-}$ myocytes (Figure 3G). Hence, the absence of MK2 did not significantly alter the Ca^{2+} content of cardiomyocyte sarcoplasmic reticulum or its capacity for Ca^{2+} release and reuptake.

Heart Rate Normalizes When Hearts From MK2$^{-/-}$ Mice Are Perfused Ex Vivo in Working Mode

To determine if the observed bradycardia involved mechanisms intrinsic to the MK2-deficient heart, we next examined heart function in isolated hearts. The heart simultaneously uses multiple substrates for energy
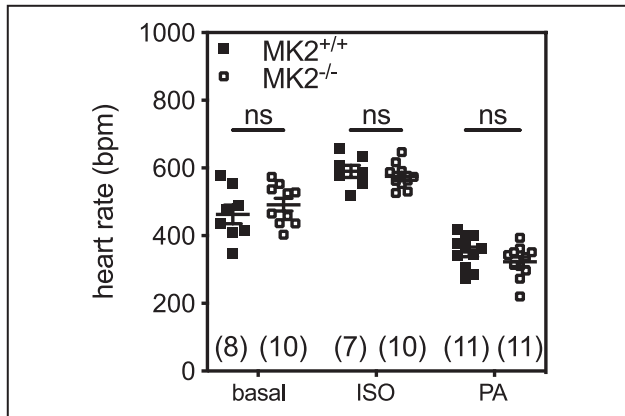
Figure 4. Heart rates do not differ significantly when MK2^+/+ and MK2^−/− hearts are perfused ex vivo.
Heart rates in isolated working hearts from MK2^+/+ and MK2^−/− mice perfused with modified Krebs-Henseleit buffer alone (basal), buffer containing 10 nmol/L isoproterenol (ISO), or 0.6 mmol/L palmitic acid (PA). Data shown are mean±SEM of 7 to 11 heart preparations. The actual number of animals per group are indicated in parentheses. MK2 indicates mitogen-activated protein kinase–activated protein kinase-2; ns, not significantly different by 2-way ANOVA with Tukey's posttests.

production[42]; hence, cardiac function was examined in the presence of (1) exogenous carbohydrates and (2) exogenous carbohydrates plus palmitate as energy sources. First, in contrast to observations of heart rate made in vivo, when hearts were perfused ex vivo in a semirecirculating working mode, heart rates in MK2^+/+ and MK2^−/− mice were similar (MK2^+/+: 463±27 beats/min, n=8; MK2^−/−: 491±19 beats/min, n=10; Table 6, Figure 4). Our assessment of heart function ex vivo included evaluating the response to isoproterenol wherein hearts from MK2^+/+ and MK2^−/− mice were perfused in working mode for 20 minutes, after which isoproterenol (10 nmol/L) was added to the perfusion buffer for an additional 20 minutes. Hearts from both MK2^−/− and MK2^+/+ mice responded to the presence of isoproterenol in the perfusate with an increase in heart rate, and this increase was of similar magnitude (Table 6, Figure 4). When perfused with buffer containing isoproterenol, values for most LV function parameters, especially related to systolic function and cardiac flow, remained unchanged in both MK2^+/+ and MK2^−/− hearts, although LV developed pressure increased significantly in MK2-deficient but not wild-type hearts. Similarly, isoproterenol induced a significant increase in the maximum rate of relaxation in MK2-deficient but not wild-type hearts compared with baseline. The mouse heart normally derives more than half of its energy requirements from fatty acid oxidation. No functional differences were observed between MK2^+/+ and MK2^−/− hearts when perfused in the presence of palmitate (0.6 mmol/L), although it is worth noting that with the addition of palmitate to the perfusing buffer, there were more functional changes in MK2-deficient

Table 7. Mitochondrial Parameters From MK2^−/− and MK2^+/+ Hearts

	MK2^+/+	MK2^−/−
n	8	8
Mitochondrial respiration, ng oxygen atoms/mg per min		
Glutamate+malate		
State 3	130±6	141±12
State 4	33.0±2.0	38.6±2.4
RCR	4.3±0.4	3.6±0.2
Pyruvate+malate		
State 3	412±17	455±24
State 4	55.2±4.7	62.0±3.2
RCR	8.2±0.6	7.4±0.5
Palmitoyl-carnitine+malate		
State 3	441±21	399±38
State 4	49.7±5.9	45.0±4.6
RCR	8.8±1.3	10.1±1.0
Succinate+rotenone		
State 3	467±29	423±26
State 4	167±18	166±15
RCR	3.7±0.7	2.7±0.2
Mitochondrial enzymatic activities		
CS activity, μmol/mg/min	1.76±0.12	1.66±0.06
MCAD activity, μmol/mg per min	0.18±0.01	0.18±0.01
SD activity, μmol/mg per min	0.015±0.001	0.020±0.001*
ICDH activity, mmol/mg per min	1.29±0.15	1.08±0.07
Mitochondrial H_2O_2 production rate, nmol/min per mg		
State 3	0.07±0.01	0.07±0.01
State 4	0.37±0.03	0.38±0.02

Data are mean±SEM. CS indicates citrate synthase; ICDH, isocitrate dehydrogenase; MCAD, medium chain acyl-CoA dehydrogenase; MK2, mitogen-activated protein kinase–activated protein kinase-2; RCR, respiratory control ratio; and SD, succinate dehydrogenase.
*$P<0.05$, MK2^+/+ vs MK2^−/−.

hearts, relative to carbohydrates alone as the exogenous energy source, than observed in wild-type hearts (Table 6). Overall, it was interesting to note that, whereas MK2-deficient hearts were bradycardic when assessed in vivo, when cardiac function was assessed ex vivo in an isolated working heart preparation, no difference in heart rate was observed.

MK2^−/−-Mice Are Characterized by Changes in Transcript Abundance for Metabolic Genes and Decreased Sensitivity for mPTP Opening

Although it is estimated that mitochondria contribute marginally to Ca^{2+} removal during global Ca^{2+} transients in healthy cardiomyocytes, mitochondria

occupy ≈30% of the volume of a cardiomyocyte and may therefore influence diastolic Ca^{2+}. In this regard, and because of the age-dependent weight loss observed in MK2-deficient mice, we examined certain aspects of mitochondria function. First, we evaluated function in isolated mitochondria by measuring oxygen consumption in state 3 and state 4. Compared with mitochondria from wild-type hearts, those from MK2$^{-/-}$ hearts showed no difference in mitochondrial respiration, irrespective of substrates used, or in mitochondrial generation of reactive oxygen species, specifically hydrogen peroxide (Table 7). However, mitochondria from MK2$^{-/-}$ hearts showed a decreased sensitivity for mPTP opening as evidenced
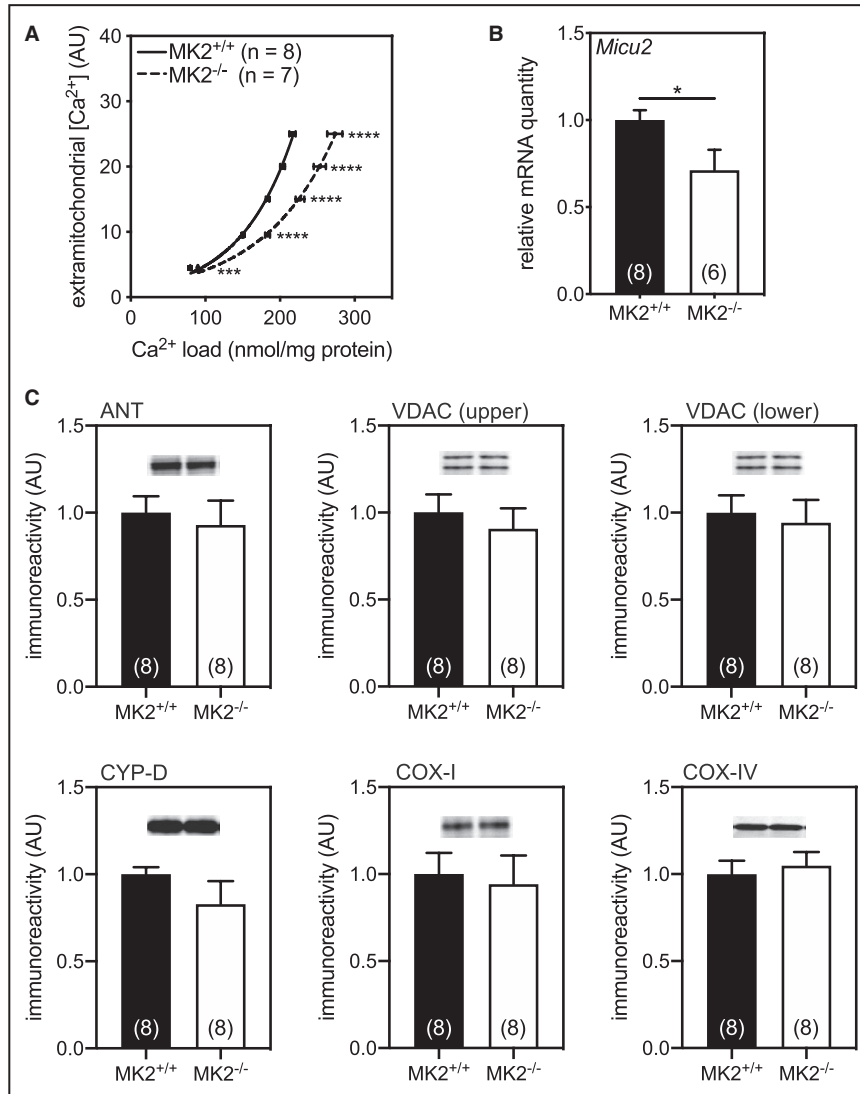
Figure 5. Calcium-sensitivity in isolated mitochondria from 12-week-old MK2$^{-/-}$ mice showed delayed mitochondrial permeability transition pore (mPTP) opening compared with their littermate counterparts.
Subsarcolemmal mitochondria were isolated from MK2$^{-/-}$ and MK2$^{+/+}$ hearts and assessed for their ability to buffer extramitochondrial calcium. **A**, Low calcium loads are sustainable by mitochondria; however, when a threshold calcium load is attained, a large and abrupt increase in extramitochondrial calcium signifies opening of the mPTP. **B**, The abundance of the mitochondrial Ca^{2+} uptake 2 (*Micu2*) mRNA, a regulatory subunit of the mitochondrial inner membrane Ca^{2+} uniporter, in the ventricular myocardium. **C**, The abundance of immunoreactivity of the different proteins responsible for mitochondrial permeability transition. Cytochrome c oxidase subunits 1 (COX-I) and 4 (COX-IV) immunoreactivity served as loading controls. Data are expressed as mean±SEM (n=8). *P<0.05, ***P<0.001, ****P<0.0001, MK2$^{+/+}$ vs MK2$^{-/-}$. ANT indicates adenine nucleotide translocase; AU, arbitrary units; CYP-D, cyclophilin-D; MK2, mitogen-activated protein kinase–activated protein kinase-2; and VDAC, voltage-dependent anion channel.
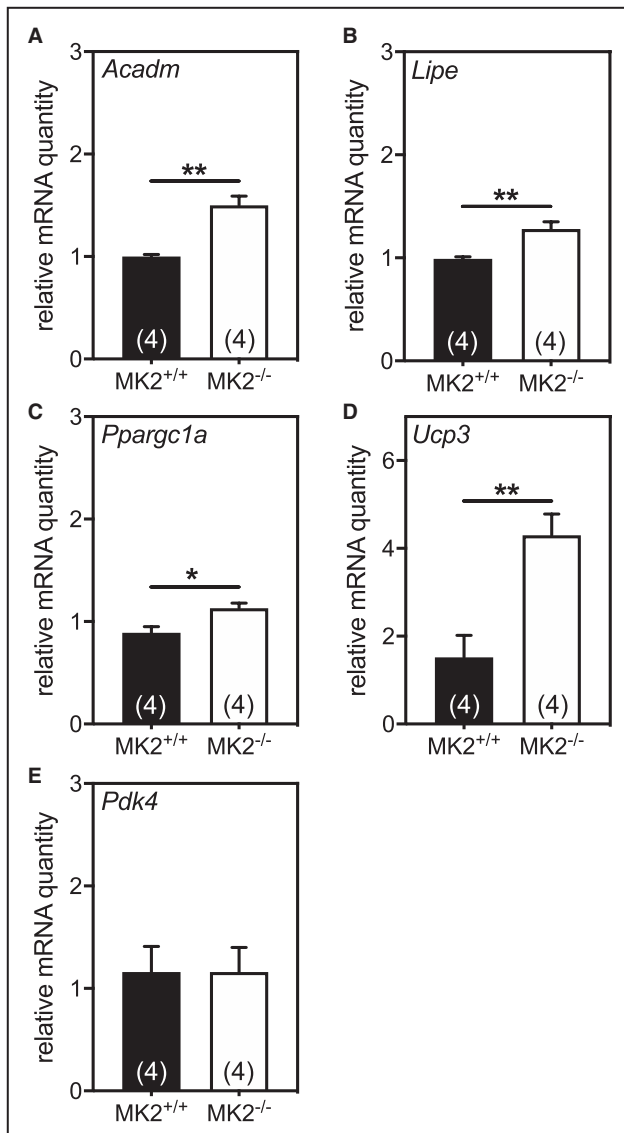
Figure 6. MK2$^{-/-}$ mice showed changes in specific mitochondrial-associated markers.
The abundance of mRNA for genes encoding (**A**) medium-chain acyl-CoA dehydrogenase (*Acadm*), (**B**) hormone-sensitive lipase (*Lipe*), (**C**) peroxisome proliferator-activated receptor γ coactivator 1α (*Ppargc1a*), (**D**) uncoupling protein 3 (*Ucp3*), and (**E**) pyruvate dehydrogenase kinase 4 (*Pdk4*) was evaluated on RNA isolated from the ventricular myocardium. Data were normalized to the abundance of *Gapdh* mRNA. Values shown were normalized to that of a representative MK2$^{+/+}$ mouse and expressed as mean±SEM. n=4 mice/group. *$P<0.05$, **$P<0.01$, MK2$^{+/+}$ vs MK2$^{-/-}$. *$P<0.05$, ** $P<0.01$, MK2$^{+/+}$ vs MK2$^{-/-}$. MK2 indicates mitogen-activated protein kinase–activated protein kinase-2.

by the greater cumulative calcium load needed to trigger mPTP opening (Figure 5A). Interestingly, this occurred despite no significant changes in the abundance of immunoreactivity of different proteins putatively involved in the cardiac mPTP complex, namely, cyclophilin-D, voltage-dependent anion channel, and adenine nucleotide translocase (Figure 5C).

Cytochrome c oxidase subunits I and 4 served as loading controls for mitochondrial protein (Figure 5C). As single-nucleotide polymorphisms in the mitochondrial calcium uptake 2 (*MICU2/EFHA1*) gene have been associated with changes in P-R segment duration,[54] transcript levels for *Micu2* were assessed by quantitative polymerase chain reaction and found to be reduced in hearts from MK2$^{-/-}$ mice (Figure 5B).

At the metabolic level, although serum glucose, free fatty acids, triglycerides, and ketone body levels did not differ between MK2$^{-/-}$ mice and MK2$^{+/+}$ mice (data not shown), the abundance of mRNAs encoding medium-chain acyl–coenzyme A dehydrogenase, hormone-sensitive lipase, peroxisome proliferator-activated receptor γ coactivator 1α (PGC1α), and uncoupling protein 3 were significantly higher in ventricular myocardium from MK2$^{-/-}$ mice compared with controls (Figure 6). In addition, the activity of mitochondrial enzymes isocitrate dehydrogenase, citrate synthase, and medium-chain acyl–coenzyme A dehydrogenase was similar between both groups, whereas that of succinate dehydrogenase activity was increased by 30% in mitochondria from MK2$^{-/-}$ hearts (MK2$^{+/+}$: 0.015±0.001 µmol/mg per minute, n=8; and MK2$^{-/-}$: 0.020±0.001 µmol/mg per minute, n=8; $P<0.05$; Table 7).

Pressure Overload–Induced Myocardial Remodeling Is Not Prevented in MK2-Deficient Mice

Given (1) the above-mentioned marginal effects of MK2 deletion on baseline cardiac function; (2) the cardioprotective effects of an MK2-deficiency in a streptozotocin model of diabetes mellitus[33]; (3) increased afterload induced by TAC both activates p38 MAPKs and increases phosphorylation of hsp25 at residues phosphorylated by MKs 2, 3, and 5 (serine-15, serine-82)[12,55]; and (4) the hypertrophic cardiomyopathy resulting from an acute, cardiomyocyte-specific activation of the p38 pathway in adult mice is attenuated by MK2 deficiency,[21] we next assessed the effect of MK2-deficiency on cardiac remodeling in response to TAC. Twelve-week-old male MK2-deficient and wild-type littermate male mice underwent TAC and were sacrificed 2 or 8 weeks after surgery, as described previously.[40] Invasive hemodynamic assessment revealed that TAC induced increases in both peak systolic arterial pressure and peak LV pressure that did not differ significantly between TAC-MK2$^{+/+}$ and TAC-MK2$^{-/-}$ groups (Table 8, Figure 7A) with an average overall increase in peak systolic arterial pressure of 40 mm Hg. In addition, echocardiographic imaging of the aortic arch revealed comparable flow velocities at the site of constriction in TAC-MK2$^{+/+}$ and TAC-MK2$^{-/-}$ groups (Table 9). Hence, an increase in afterload was similarly established in both

Table 8. Hemodynamic Parameters for MK2$^{+/+}$ and MK2$^{-/-}$ Mice 2 and 8 Weeks After TAC

	2 wk				8 wk			
	Sham Operation		TAC		Sham Operation		TAC	
	MK2$^{+/+}$	MK2$^{-/-}$	MK2$^{+/+}$	MK2$^{-/-}$	MK2$^{+/+}$	MK2$^{-/-}$	MK2$^{+/+}$	MK2$^{-/-}$
n	8	8	11	10	11	11	9	9
BP$_{max}$, mm Hg	99.4±5.3	89.4±2.9	129±9	139±10*	88.4±4.0	82.0±2.3	122±8†	129±11*
LVP$_{max}$, mm Hg	103±8	90.5±2.2	139±11	143±12†	94.4±3.8	89.5±2.2	121±8‡	138±11§
LVP$_{min}$, mm Hg	3.3±0.9	4.3±0.9	4.8±1.8	3.5±1.3	0.7±0.6	1.2±0.4	2.8±1.5	0.9±0.5
+dP/dt, mm Hg/s	5713±257	4571±254	6355±441	5788±525	6330±401	6458±551	5586±416	6589±420
−dP/dt, mm Hg/s	5336±294	4308±221	6500±629	6823±753‡	6829±313	6508±258	6848±681	8450±560‡,∥
LVEDP, mm Hg	8.7±1.3	10.0±1.3	10.4±2.2	9.2±1.4	4.8±0.7	6.0±0.7	7.2±1.8	5.6±0.7
CT, ms	13.4±0.4	14.9±0.7	14.3±0.6	14.6±1.2	11.6±0.2	10.7±0.3	11.5±0.5	11.3±0.4
RT, ms	46.1±0.9	50.2±0.7¶	43.5±0.8	43.2±0.8§,∥	40.6±0.5	39.7±0.5	41.9±1.4	38.9±0.5
Tau, ms	7.4±1.2	9.1±1.4	4.3±1.2	4.5±1.5	6.6±0.3	6.3±0.1	8.0±1.0	6.0±0.2
HR, beats/min	368±24	301±13	389±19	349±8	422±10	421±14	423±12	436±17

Data are expressed as mean±SEM. For statistical comparisons 2-way ANOVA followed by Tukey's multiple comparison test was performed. BP$_{max}$ indicates maximum systolic blood pressure; CT, contraction time; +dP/dt, maximum rate of left ventricular pressure increase during contraction; -dP/dt, maximum rate of left ventricular decline during relaxation; HR, heart rate; LVEDP, left ventricular end-diastolic pressure; LVP$_{max}$, left ventricular maximum systolic pressure; LVP$_{min}$, left ventricular minimum diastolic pressure; MK2, mitogen-activated protein kinase–activated protein kinase-2; RT, relaxation time; *T*, time constant; and TAC, transverse aortic constriction.

*P<0.001 vs sham.
†P<0.01 vs sham.
‡P<0.05 vs sham.
§P<0.0001 vs sham.
∥Indicates a significant interaction between the effects of TAC and genotype; P<0.05.
¶P<0.05 vs MK2$^{+/+}$.

MK2$^{+/+}$ and MK2$^{-/-}$ mice. Two weeks after TAC, echocardiographic imaging revealed LV mass increased by 47% (sham: 103±3 mg, n=17; TAC: 151±8 mg, n=16; P<0.0001) in MK2$^{+/+}$ mice, which was attenuated to an increase of 9% in MK2-deficient mice that did not reach statistical significance (sham: 112±6 mg, n=14; TAC: 128±7 mg, n=15; P>0.05). Similarly, heart weight to tibia length ratios were increased by 37% in MK2$^{+/+}$ (sham: 67.9±3.9 mg/cm, n=8; TAC: 92.8±5.1 mg/cm, n=11; P<0.001) and by only 7.8% in MK2$^{-/-}$ mice (sham: 66.9±3.8 mg/cm, n=10; TAC: 77.1±2.1 mg/cm, n=10; P>0.05; Figure 7B). Pathological LV hypertrophy is associated with molecular remodeling that includes the reexpression of the cardiac fetal genes atrial natriuretic peptides (*Nppa*) and β-myosin heavy chain (*Myh7*).[56] *Nppa* and *Myh7* mRNA levels were quantified by quantitative polymerase chain reaction 2 weeks after TAC. Although hypertrophy was significant in MK2$^{+/+}$ but not MK2$^{-/-}$ mice 2 weeks after TAC, *Nppa* (Figure 8A) and *Myh7* (Figure 8B) mRNA levels in MK2$^{+/+}$ and MK2$^{-/-}$ hearts increased to similar levels. Eight weeks after TAC, LV mass was similarly increased in MK2$^{+/+}$ mice by 64% (sham: 106±3 mg, n=11; TAC: 174±14 mg, n=11; P<0.0001) and in MK2$^{-/-}$ mice by 50% (sham: 109±3 mg, n=11; TAC: 164±8 mg, n=10; P<0.001) (Table 9). Similarly, 8 weeks after TAC, LV myocyte diameter in MK2$^{+/+}$ and MK2$^{-/-}$ hearts did not differ significantly (data not shown). Hence, although LV

hypertrophy was not significant in MK2-deficient mice 2 weeks after TAC, the absence of MK2 did not prevent hypertrophy in response to a chronic increase in afterload.

Direct hemodynamic assessment by Millar catheter did not reveal major functional differences between TAC-MK2$^{+/+}$ and TAC-MK2$^{-/-}$ mice; however, at both 2 and 8 weeks after TAC, MK2-deficient hearts showed a significant increase in the maximum rate of relaxation relative to sham MK2$^{-/-}$ mice, whereas MK2$^{+/+}$ mice did not (Table 8). Assessment of LV structure and function by echocardiographic imaging 2-weeks after TAC revealed reduced end-diastolic diameter in TAC MK2$^{-/-}$ mice compared with both their sham counterparts (sham: 4.14±0.07 mm, n=14; TAC: 3.84±0.07 mm, n=15; P<0.05) and TAC MK2$^{+/+}$ mice (4.18±0.08 mm, n=16; P<0.01 versus TAC MK2$^{-/-}$). Eight weeks after TAC, these differences were no longer significant. LV anterior and posterior wall thicknesses were increased to a similar extent in both TAC MK2$^{+/+}$ and TAC MK2$^{-/-}$ mice (≈20%; P<0.001; Table 9). LV ejection fraction was reduced in MK2$^{+/+}$ mice 2 weeks after TAC (sham: 68.8±1.8%, n=17; TAC: 59.9±3.0%, n=16; P<0.05), whereas it was increased in MK2$^{-/-}$ mice (sham: 64.4±2.0%, n=14; TAC: 73.6±1.4%, n=15; P<0.05) with left ventricular ejection fraction being 23% greater in TAC MK2$^{-/-}$ mice than TAC MK2$^{+/+}$ mice (P<0.001). Although these
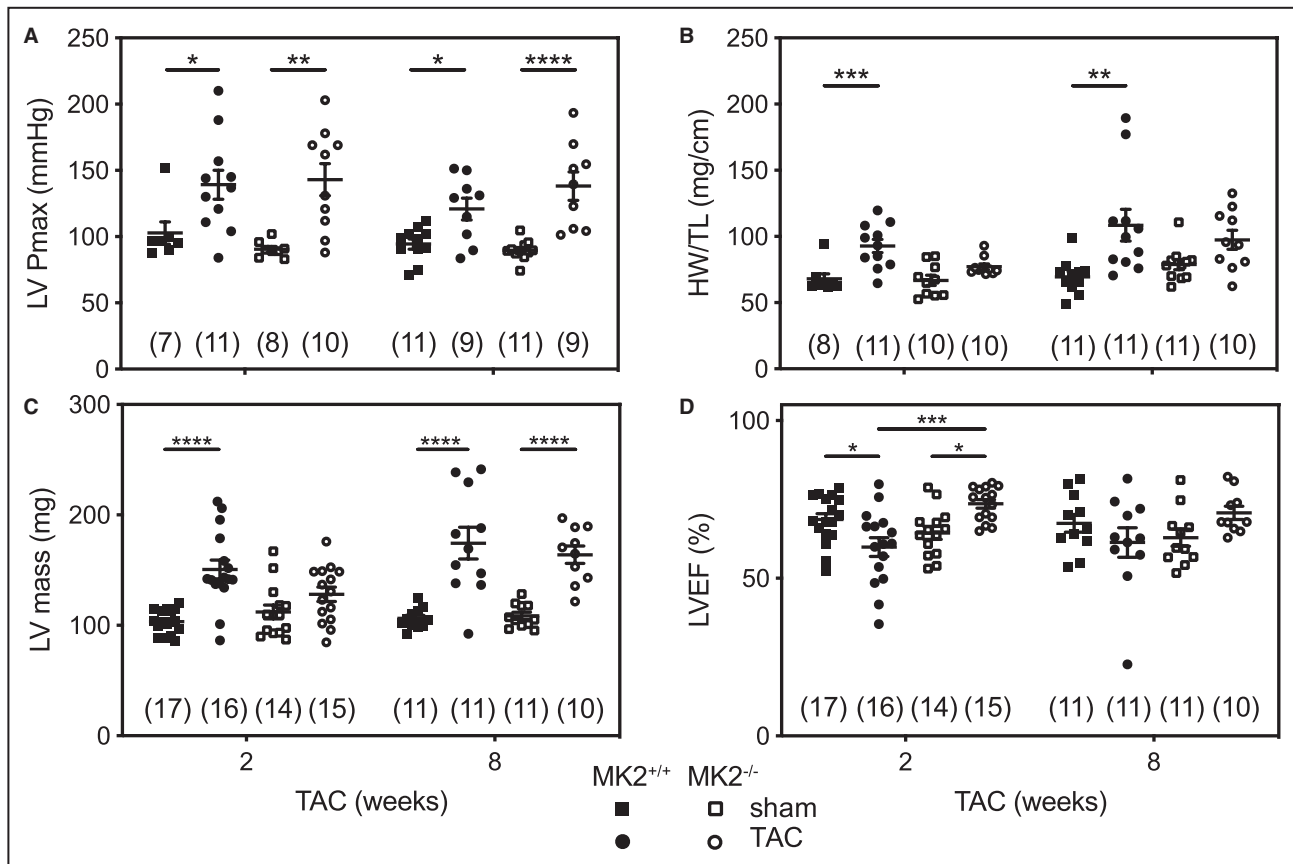
Figure 7. **Hypertrophy is delayed in MK2$^{-/-}$ hearts subjected to transverse aortic constriction (TAC).**
Pressure overload was induced in MK2$^{-/-}$ and wild-type littermate control (MK$^{+/+}$) mice by TAC, and mice were euthanized 2 and 8 weeks after surgery. Sham-operated (sham) animals underwent the identical surgical procedure; however, the aorta was not constricted. Left ventricular (LV) maximum developed pressure (LVPmax; **A**), heart weight–to–tibia length ratio (HW/TL; **B**), LV mass (**C**), and left ventricular ejection fraction (LVEF, **D**). Heart weight refers to the mass of the whole heart (minus atria) as determined gravimetrically. LV mass was determined by echocardiography. Data are expressed as means±SEM. *P<0.05, **P<0.01, ***P<0.001, and ****P<0.001 by 2-way ANOVA with Tukey's multiple-comparison posttest. Number of animals per group are indicated in parentheses. MK2 indicates mitogen-activated protein kinase–activated protein kinase-2.

differences were also observed 8 weeks after TAC, they did not reach statistical significance. However, 2-way ANOVA indicated a significant interaction between the effects of TAC and genotype on LV diameter (LV end-diastolic diameter, LV dimension at end cardiac systole), LV mass, and LV function (LV ejection fraction, LV fractional shortening) 2-weeks after TAC (Table 9). Specifically, whereas LV diameter increased and ejection fraction decreased in MK2$^{+/+}$ mice, the opposite was observed in MK2-deficient mice. Furthermore, a significant interaction between the effects of TAC and genotype on LV ejection fraction and LV fractional shortening was also observed 8 weeks after TAC.

Systolic and early diastolic tissue velocity at the basal segments of the interventricular septum and lateral LV wall was assessed by tissue Doppler imaging. As mentioned above, both lateral and septal systolic tissue velocities were lower in 12-week-old MK2$^{-/-}$ mice relative to MK2$^{+/+}$ mice (Table 2). Two weeks after

TAC, systolic tissue velocities in TAC MK2$^{-/-}$ mice did not differ from those in sham MK2$^{-/-}$ mice (Table 9). In contrast, 2 weeks after TAC, lateral and septal systolic tissue velocities were significantly lower in TAC MK2$^{+/+}$ relative to sham MK2$^{+/+}$ mice. However, no differences in systolic tissue velocities were observed 8 weeks after TAC (Table 9). Two-way ANOVA indicated a significant interaction between the effects of TAC and genotype on both systolic and early diastolic tissue velocities (as well as E/E$_m$ and E$_m$/A$_m$), in both septal and lateral segments, 2 weeks after TAC.

Early and late transmitral flow velocities, as well as the E/A ratio, did not differ significantly between TAC MK2$^{+/+}$ and TAC MK2$^{-/-}$ mice either 2 or 8 weeks after TAC (Table 9). The E wave deceleration time and rate-corrected isovolumetric relaxation time were shortened significantly, relative to sham, in TAC MK2$^{-/-}$ mice but not in TAC MK2$^{+/+}$ mice 8 weeks after TAC (Figure 9A and 9B). Although these changes suggest LV compliance was reduced in TAC MK2$^{-/-}$ mice, E

Table 9. Echocardiographic Parameters of MK2+/+ and MK2−/− Mice 2 and 8 Weeks After TAC

	2 wk				8 wk			
	Sham		TAC		Sham		TAC	
	MK2+/+	MK2−/−	MK2+/+	MK2−/−	MK2+/+	MK2−/−	MK2+/+	MK2−/−
n	17	14	16	15	11	11	11	10
Aortic peak velocity, cm/s	70.5±5.3	74.8±3.8	305±16*	293±21*	79.1±4.0	72.9±2.7	340±11*	330±22*
R-R interval, ms	151±5	184±14†	148±5	175±7‡	150±7	173±8	137±6	146±7
LV structure								
LVAW$_d$, mm	0.740±0.012	0.743±0.015	0.932±0.030*	0.914±0.039§	0.725±0.004	0.0734±0.020	0.977±0.046*	1.025±0.033*
LVPW$_d$, mm	0.701±0.013	0.718±0.020	0.870±0.027*	0.863±0.019*	0.708±0.009	0.736±0.020	0.932±0.036*	0.942±0.025*
LVD$_d$, mm	4.00±0.06	4.14±0.07	4.18±0.08	3.84±0.07†||¶	4.10±0.05	4.08±0.08	4.34±0.15	4.10±0.05
LVD$_s$, mm	2.57±0.09	2.76±0.10	2.73±0.12	2.47±0.10¶	2.75±0.10	2.88±0.12	3.10±0.23	2.66±0.08
LV mass, mg	103±3	112±6	151±8*	128±7¶	106±3	109±3	174±14*	164±8§
LV mass/LVD$_d$, mg/mm	25.8±0.5	26.9±1.2	35.8±1.6*	33.3±1.4#	25.9±0.4	26.6±0.7	39.8±2.5*	39.9±1.7*
LV mass/BW, mg/g	3.78±0.10	4.06±0.18	5.36±0.29*	5.14±0.22#	3.24±0.18	3.06±0.12	5.58±0.71*	4.89±0.28§
LV systolic function								
LVFS, %	33.5±1.3	30.5±1.4	27.9±1.9||	37.2±1.1||,¶,**	33.2±2.1	29.6±1.9	29.2±2.8	35.1±1.7¶
LVEF, %	68.6±1.8	64.4±2.0	59.3±3.0||	73.6±1.4||,¶,**	67.4±2.8	62.9±2.7	61.4±4.7	70.7±2.1¶
Lateral S$_m$, cm/s	2.17±0.11	1.81±0.09	1.66±0.07†||	1.88±0.15¶	2.00±0.12	1.71±0.08	1.69±0.11	1.59±0.10
Septal S$_m$, cm/s	2.33±0.11	1.85±0.08‡	1.88±0.11||	1.98±0.13¶	2.27±0.11	1.87±0.08	2.05±0.17	1.95±0.06
Transmitral flow								
E velocity, cm/s	79.3±1.8	78.9±3.1	92.4±3.9||	91.4±4.5	86.0±2.6	89.8±3.4	104±3||	102±6
E DT, ms	37.7±2.0	41.0±1.5	34.7±2.0	36.2±2.1	35.4±1.2	37.9±1.3	32.6±2.0	29.7±1.5#
ED rate, m/s²	21.9±1.1	19.6±1.1	28.0±2.0	26.8±2.5||	24.7±1.4	23.9±1.0	32.9±2.2||	35.0±2.5§
A velocity, cm/s	45.8±3.5	50.4±1.4	51.1±6.4	51.9±4.7	50.8±3.0	41.6±3.1	49.1±4.0	49.2±2.8
E/A	1.76±0.15	1.56±0.07	2.01±0.53	1.96±0.26	1.75±0.10	2.34±0.26	2.15±0.21	2.18±0.23
Lateral E$_m$, cm/s	2.91±0.26	2.06±0.18‡	2.15±0.24	2.50±0.18¶	2.37±0.19	2.16±0.16	2.71±0.16	2.59±0.23
Lateral A$_m$, cm/s	2.53±0.14	2.47±0.23	2.20±0.36	2.04±0.29	2.50±0.20	1.88±0.08‡	2.16±0.15	1.78±0.15
Lateral E$_m$/A$_m$	1.13±0.11	0.908±0.119	0.668±0.018	1.52±0.22||¶	0.977±0.085	1.16±0.08	1.31±0.13	1.53±0.15
Lateral E/E$_m$	29.2±2.6	40.6±4.0	45.5±8.3||	39.0±2.8||	38.0±3.9	43.3±3.6	40.0±2.5	41.8±3.9
Septal E$_m$, cm/s	3.10±0.29	2.19±0.22‡	2.38±0.32	2.86±0.16¶	2.48±0.15	2.50±0.09	3.00±0.23	2.77±0.17
Septal A$_m$, cm/s	2.71±0.18	2.27±0.13	2.53±0.57	1.95±0.24	2.58±0.14	2.04±0.09‡	2.27±0.14	1.86±0.14
Septal E$_m$/A$_m$	1.06±0.08	0.975±0.077	0.883±0.110	1.71±0.19§||	1.00±0.10	1.24±0.07	1.38±0.17	1.57±0.17
Septal E/E$_m$	27.3±2.2	38.2±2.9‡	41.4±6.2||	33.1±2.1¶	35.7±2.4	36.3±2.2	36.8±3.0	37.5±2.5

(Continued)

Table 9. Continued

	2 wk				8 wk			
	Sham		TAC		Sham		TAC	
	MK2+/+	MK2−/−	MK2+/+	MK2−/−	MK2+/+	MK2−/−	MK2+/+	MK2−/−
LV isovolumetric relaxation time								
IVRT, ms	13.3±1.1	15.4±1.3	13.5±1.2	14.3±1.9	8.63±0.59	11.2±1.1	7.26±0.53	6.92±1.3#
IVRTc, ms	1.08±0.09	1.13±0.10	1.10±0.09	1.08±0.14	0.700±0.034	0.838±0.065	0.625±0.047	0.561±0.089#
LADs, mm	2.55±0.05	2.44±0.04	2.79±0.10	2.43±0.06†	2.53±0.06	2.50±0.05	2.86±0.10‖	2.62±0.07
Pulmonary venous flow								
Upper S/D	0.465±0.043	0.534±0.063	0.332±0.030	0.537±0.106	0.635±0.039	0.453±0.054	0.464±0.046	0.515±0.069¶
Lower S/D	1.79±0.14	1.67±0.13	2.13±0.21	1.70±0.10	1.62±0.13	1.62±0.14	1.98±0.18	2.00±0.14
S/D slope	5.57±0.35	6.53±0.47‡	3.93±0.26	5.20±0.46‡	5.48±0.43	6.28±0.66	4.00±0.13	4.45±0.40‡
MPI								
Septal MPI, %	83.9±8.2	81.5±5.7	96.2±10.1	78.7±13.5	58.7±2.4	60.4±1.9	61.7±11.7	46.4±2.9
Lateral MPI, %	86.9±8.2	91.2±8.6	99.2±9.9	78.5±12.7	56.9±1.7	58.5±2.5	63.1±8.0	44.7±3.2†‖¶
Global MPI, %	54.6±3.0	56.5±3.4	55.0±5.0	38.4±5.1¶	40.0±2.2	47.8±2.4	43.4±8.0	33.5±2.1‖

Data are expressed as mean±SEM. A indicates transmitral flow late (atrial) filling velocity; A_m, mitral annulus peak velocity during atrial diastolic filling; CO, cardiac output; D, peak velocity during pulmonary venous diastolic flow; E, transmitral flow early filling velocity; ED, E wave deceleration; EDT, E wave deceleration time; E_m, mitral annulus peak velocity during early diastolic filing; IVRT, isovolumic relaxation time; IVRTc, heart rate-corrected IVRT; LAD_d, left atrium dimension at end cardiac diastole; LAD_s, left atrium dimension at end cardiac systole; $LVAW_d$, left ventricular anterior wall thickness at end cardiac diastole; LVD_d, left ventricular dimension at end cardiac diastole; LVD_s, left ventricular dimension at end cardiac systole; LVEF, left ventricular ejection fraction; LVFS, left ventricular fractional shortening; $LVPW_d$, left ventricular posterior wall thickness at end cardiac diastole; LVV_d, left ventricular volume at end cardiac diastole; LVV_s, left ventricular volume at end cardiac systole; MK2, mitogen–activated protein kinase–activated protein kinase-2; MPI, myocardial performance index; S, peak velocity during pulmonary venous systolic flow; SD slope, pulmonary venous systolic flow decelerating slope; S_L, basal lateral systolic velocity; S_S, basal septal systolic velocity; and SV, stroke volume.

*$P<0.0001$ vs sham.
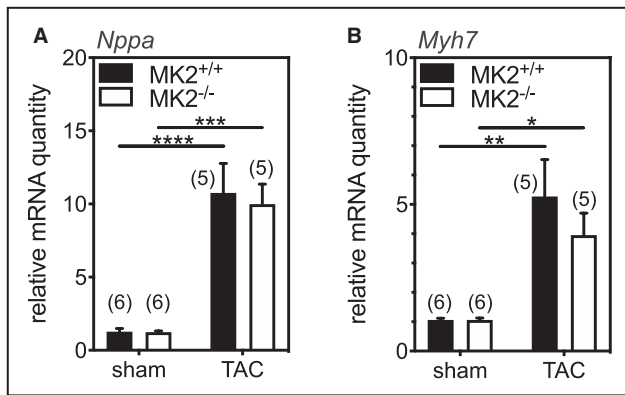
†$P<0.01$ vs MK2+/+.

‡$P<0.05$ vs MK2+/+.

§$P<0.001$ vs sham.

‖$P<0.05$ vs sham.

¶Indicates a significant interaction between the effects of TAC and genotype, $P<0.05$.

#$P<0.01$ vs sham.

**$P<0.001$ vs MK2+/+.

Figure 8. MK2 deficiency does not alter the transverse aortic constriction (TAC)-induced increase in fetal gene expression. Pressure overload was induced in MK2$^{-/-}$ and wild-type littermate control (MK2$^{+/+}$) mice by TAC, and mice were euthanized 2 weeks after surgery. Sham animals underwent the identical surgical procedure; however, the aorta was not constricted. Total RNA was isolated and the abundance of (**A**) atrial natriuretic peptide (*Nppa*) and (**B**) β-myosin heavy chain (*Myh7*) mRNA was quantified by quantitative polymerase chain reaction and normalized to *Gapdh* mRNA levels. Data are expressed as means±SEM. Number of animals per group are indicated in parentheses. *$P<0.05$, **$P<0.01$, ***$P<0.001$, and ****$P<0.001$ by two-way ANOVA with Tukey's multiple-comparison posttest. MK2 indicates mitogen-activated protein kinase–activated protein kinase-2.

wave deceleration time and rate-corrected isovolumetric relaxation time in TAC MK2$^{-/-}$ mice did not differ significantly from TAC MK2$^{+/+}$ mice. In addition, both septal and lateral E/E$_m$ ratios, which reflect LV filling pressure, did not differ. Similarly, the ratio of peak systolic to diastolic pulmonary venous flow velocity, which would increase in response to reduced LV compliance, was similar in TAC MK2$^{+/+}$ and TAC MK2$^{-/-}$ mice both 2 and 8 weeks after TAC. Furthermore, LA diameter, which may increase in response to a chronic increase in LV filling pressure,[57] increased in TAC MK2$^{+/+}$ but not TAC MK2$^{-/-}$ mice (Figure 9C). Finally, the myocardial performance index, which increases as cardiac performance is reduced, was reduced in TAC MK2$^{-/-}$ mice relative to both TAC MK2$^{+/+}$ and sham MK2$^{-/-}$ mice 2 weeks after TAC, although the difference between MK2$^{+/+}$ and MK2$^{-/-}$ mice no longer reached significance 8 weeks after TAC (Figure 9D). Two-way ANOVA indicated a significant interaction between the effects of TAC and genotype on global myocardial performance index 2-weeks post-TAC and on lateral myocardial performance index 8 weeks after TAC (Table 9). Hence, MK2-deficiency resulted in a delay in hypertrophy and the onset of the changes in LV structure and function evoked by a chronic increase in afterload.

Remodeling of the myocardium in response to a chronic increase in afterload involves both hypertrophy and increased interstitial fibrosis. We previously observed a modest fibrotic effect in mice on the mixed 129/Ola×C57BL/6 genetic background.[40] Similarly, 8 weeks after TAC, Masson's trichrome staining revealed very little increased interstitial fibrosis in TAC MK2$^{+/+}$ and TAC MK2$^{-/-}$ mice relative to their respective sham controls (Figure 10).

TAC activates the p38 pathway, with a peak activation occurring 3 days after TAC.[12,55] Furthermore, pharmacologic inhibition of p38α/β potentiates ERK1/2 activation in cardiac myocytes.[58] Hence, we examined the effects of MK2-deficiency and TAC on phosphorylation of p38, MEK1/2, and ERK1/2 within their activation loops. Two weeks after TAC, ERK1/2, MEK1/2 and p38 phosphorylation (normalized to total immunoreactivity) in TAC and sham hearts did not differ significantly. In each case, a modest but not significant reduction in phosphorylation was observed in the samples from MK2-deficient hearts (data not shown). In addition, MK2 deficiency has been shown previously to destabilize p38α leading to a reduction p38α immunoreactivity.[33,59] The abundance of p38α immunoreactivity was reduced in MK2-deficient hearts to a similar extent in sham and TAC hearts 2 weeks after TAC (data not shown).

DISCUSSION

Deletion of MK2 in mice had no detrimental impact on survival when examined up to 100 weeks of age. Interestingly, relative to age- and sex-matched littermates, MK2-deficient mice were hypothermic and had significantly lower body weight in later life. At 12 weeks of age, male MK2-deficient mice displayed prolonged R-R intervals as well as signs of early diastolic dysfunction; however, diastolic dysfunction failed to develop with age. The amplitude and decay of calcium transients evoked by either field stimulation or caffeine were similar in ventricular myocytes isolated from adult male MK2$^{+/+}$ and MK2$^{-/-}$ mice, whereas when perfused ex vivo, in working mode, hearts from MK2$^{+/+}$ and MK2$^{-/-}$ mice beat with similar frequency. Acquisition of ECG data in conscious mice by radio telemetry revealed P-R segment prolongation in MK2-deficient mice, suggesting that autonomic regulation of heart function was altered in these mice. Finally, the LV hypertrophy induced by imposing a chronic increase in afterload was delayed but not prevented in MK2-deficient mice.

Echocardiographic imaging in 12-week-old male MK2$^{-/-}$ mice revealed signs of reduced LV compliance, suggesting early diastolic dysfunction. However, MK2-deficient mice failed to develop diastolic dysfunction as they aged. Several factors are known to affect diastolic function, including preload,[60] aging,[61] and heart rate.[62] Although in theory the observed changes in diastolic function in MK2-deficient mice could be related to a decrease in heart rate, isovolumetric relaxation time in
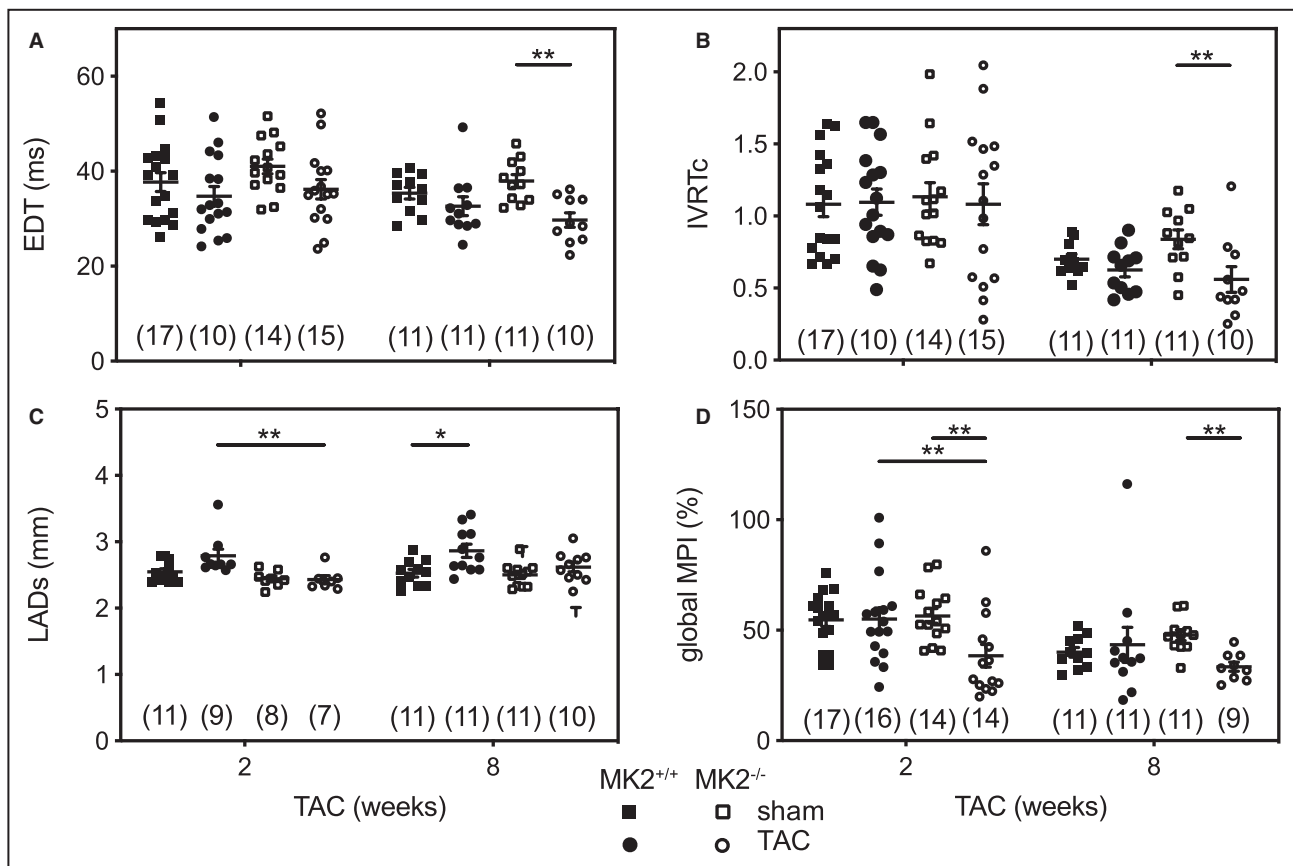
Figure 9. MK2-deficient hearts are not predisposed to further diastolic dysfunction when challenged with a chronic increase in afterload.
Pressure overload was induced in MK2−/− and wild-type littermate control (MK+/+) mice by constriction of the transverse aorta (TAC), and mice were euthanized 2 and 8 weeks after surgery. Sham-operated (sham) animals underwent the identical surgical procedure; however, the aorta was not constricted. **A**, E wave deceleration time (EDT), (**B**) isovolumetric relaxation time corrected for differences in R-R interval (IVRTc), (**C**) left atrial diameter at systole (LAD$_s$), and (**D**) global myocardial performance index (MPI: note that higher values indicate poorer cardiac function). Data are presented as means±SEM. *$P<0.05$, **$P<0.01$ by two-way ANOVA with Tukey's multiple-comparison posttest. Number of animals per group are indicated in parentheses. MK2 indicates mitogen-activated protein kinase–activated protein kinase-2.

MK2−/− mice was significantly longer than MK2+/+ mice even after being corrected for heart rate. Among clinical strategies used to improve diastolic function, treatments such as beta blockers have been employed to both decrease heart rate and increase diastolic filling time.[63] Hence, one possible explanation for the lack of progression to diastolic dysfunction in MK2−/− mice could be a protective effect resulting from reduced heart rate.

Although bradycardic in vivo, when hearts from wild-type and MK2-deficient mice were assessed using an ex vivo working heart preparation, heart rates did not differ, as shown previously.[33] This discrepancy can be explained by the nonnegligible impact of differences in body temperature, neuronal, and hormonal regulation that would be absent in ex vivo heart preparations. Possible mechanisms involved in lowering the heart rate in MK2-deficient mice include changes in autonomic regulation of heart function: an enhanced parasympathetic regulation or a decreased

sympathetic regulation could reduce heart rate.[64] Consistent with this, when ECGs were acquired from conscious mice using radio telemetry, prolonged R-R intervals were observed in MK2-deficient mice along with prolongation of the P-R segment with no change in the P wave–to–QRS complex ratio. These observations are also consistent with there being alterations in autonomic regulation of heart function in the MK2-deficient mice. However, this hypothesis is based on basic functional observations, and further investigations will be required to better understand the role of MK2 in parasympathetic and sympathetic regulation of cardiac function, including the conduction velocity within the atrioventricular node, and the G protein–coupled receptors involved in the catecholaminergic control of heart rate and contractility.[65] Overall, the above-mentioned results suggest a novel role for MK2 in regulating heart rate and diastolic function and highlight a new putative therapeutic target for
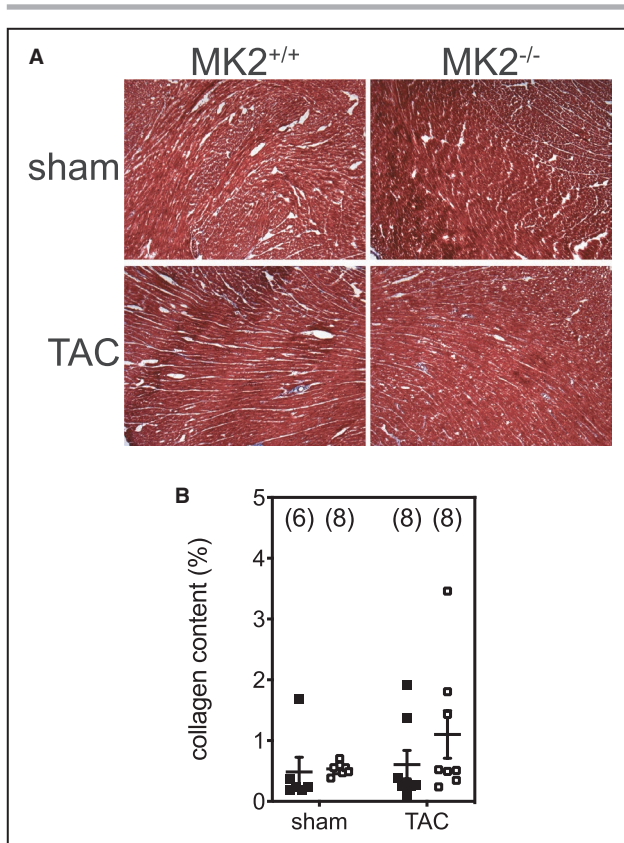
Figure 10. MK2 deficiency had no effect on interstitial fibrosis.
A, Transverse cryosections (8 mm) of the ventricular myocardium were stained with Masson's trichrome 8 weeks after TAC. **B**, collagen content was quantified by color segmentation. The original magnification was ×40. Data are expressed as means±SEM. Number of animals per group are indicated in parentheses. MK2 indicates mitogen-activated protein kinase–activated protein kinase-2; and TAC, transverse aortic constriction.

heart diseases involving LV diastolic dysfunction. Similarly, we recently reported that a deficiency in MK2 protects mice against diabetes mellitus–induced cardiac diastolic dysfunction.[33]

Mitochondria play a central role in cardiac energy production and transduction since mitochondrial oxidative phosphorylation is responsible for roughly 90% of the ATP production in the cardiomyocyte. A close link between mitochondrial failure and cardiac remodeling and dysfunction has been illustrated in various genetic models, particularly in mouse models lacking transcriptional coactivators and key drivers of mitochondrial biogenesis and function,[66] such as PGC-1α,[67] PGC-1β,[68] or both.[69] A similar link has been established in mouse[70] and in rat[71] models of heart failure as well as in the human failing heart following ischemic heart disease or dilated cardiomyopathy.[72] In fact, heart failure is characterized by alterations in energy metabolism that include changes in substrate use for energy production, particularly

depressed fatty acid use, as well as changes in the expression of molecular regulators involved in the PGC-1α/peroxisome proliferator-activated receptor-α axis.[73,74] Therefore, targeting mitochondria in heart diseases, especially heart failure, through induction of modulators of mitochondrial biogenesis, for example, remains an active field of research aimed at identifying new therapeutic strategies.[75] In MK2-deficient mice, despite no significant changes in mitochondrial respiration rates and the activity of mitochondrial enzymes, other than succinate dehydrogenase, we observed an intriguing increase in the expression of key metabolic genes including PGC-1α and genes involved in fatty acid metabolism. MK2 has been shown to regulate the stability of mRNAs containing adenylate-uridylate–rich elements,[30,76] which could explain at least part of the changes. Based on the role of depressed PGC-1α and fatty acid–related metabolic genes in mitochondrial dysfunction in heart failure, the fact that MK2-deficient mice exhibited enhanced expression of these latter genes and improved diastolic function, suggest that MK2 could be considered as an attractive target to improve mitochondrial function in heart diseases. Similar alterations in gene expression have been observed in skeletal muscle from mice where both MK2 and MAPK-activated protein kinase-3 have been deleted.[77] However, the implication of uncoupling protein in heart failure is more controversial.[78,79] Our results on uncoupling protein expression, including uncoupling protein 3, which was increased in MK2-deficient mice, are more conflicting since some evidence supports a maladaptive effect of uncoupling proteins as key uncouplers of mitochondrial oxidative phosphorylation that decrease energetic efficiency[80] while other studies pointed to an adaptive phenomenon of uncoupling proteins in response to lipid accumulation as exporters of fatty acids[81] and by their ability to prevent reactive oxygen species accumulation and cardiomyocyte apoptosis.[78] Therefore, the significance of our findings needs to be further clarified and the metabolic profile of MK2-deficient hearts under conditions of stress assessed.

Among mechanisms involved in mitochondrial pathogenesis is the opening of the mPTP.[82,83] The exact molecular identity of this complex has not yet been well defined and is the subject of intense debate, although the molecular structure of mPTP includes the voltage-dependent anion channel, the adenine nucleotide translocator, and cyclophilin D, among other possible components that include the F1F0 ATP synthase for the pore-forming component.[82,84] Nevertheless, increased or sustained mPTP opening subsequent to reactive oxygen species or Ca^{2+} overload is involved in mitochondrial membrane permeabilization, which in turn results in mitochondrial respiratory chain uncoupling

as well as impaired oxidative phosphorylation, blunted ATP production, and ultimately mitochondrial swelling and cell death.[83,85] There is increasing evidence supporting a role for mPTP opening in cardiac diseases. In ischemia-reperfusion injury, prolonged mPTP opening has been described as a key contributor to postischemia/reperfusion-mediated cardiomyocyte death.[86] Similarly, in response to volume overload, mitochondrial vulnerability to mPTP opening increased during compensated ventricular hypertrophy.[87,88] In rats subjected to coronary artery ligation, mPTP opening was prolonged during myocardial infarction.[89] Finally, mPTP opening appears to persist in failing hearts following chronic pacing or postinfarction remodeling in dogs[90] as well as in rats following decompensated hypertrophy secondary to TAC-induced increased afterload.[91] Therefore, targeting mPTP opening is now considered to be a promising therapeutic target for the treatment of cardiac diseases and new strategies aimed at limiting mPTP opening are required to overcome the existing challenges that limit the development of specific mPTP inhibitors.[84,92] Our results show that inhibiting MK2 signaling reduced the Ca^{2+} sensitivity for mPTP opening; hence, MK2 or its downstream targets may warrant consideration in the development novel cardioprotective therapies.

When the effects of a chronic increase in afterload on cardiac remodeling were examined in MK2-deficient mice, the findings were consistent with those of Streicher et al.[21] By inducing the overexpression of a constitutively-active form of MKK3 (MKK3E) in a cardiomyocyte-specific manner, these authors showed that MK2 participates in the p38-mediated pathological cardiac remodeling and contractile dysfunction. In addition, a deficiency of MK2 attenuates ventricular hypertrophy and improves contractility, despite no difference in the expression molecular markers of remodeling. Similarly, our results show that following TAC, MK2-deficient mice took longer to develop sigificant levels of hypertrophy while showing improved contractility, despite no difference in the expression of hypertrophic markers. More specifically, 2-weeks after TAC, MK2-deficient mice showed improved (1) LV systolic function as well as (2) LV diastolic properties. These findings do not entirely concur with the findings of Streicher et al, who further showed that knocking out MK2 in MKK3E-overexpressing hearts does not rescue myocardial stiffness.[21] This discrepancy can be explained by the different model used: chronic activation of p38 MAPK versus TAC-induced increased afterload. Being a downstream target of p38α/β, MK2 could be contributing to the pathogenic responses of p38 activation by either modulating total p38α protein levels or mediated downstream signaling. In fact, in MK2-deficient mice, the amount of p38α is significantly

reduced,[33] since MK2 stabilizes p38α via a direct interaction with its C-terminal.[59] Alternatively, downstream targets of MK2, such as hsp25/27, may mediate molecular events induced by MK2 activation. Overexpression of a nonphosphorylatable hsp27 mutant improves cardiac performance.[93] However, it is noteworthy that the benefits of MK2 loss observed 2 weeks after TAC were less pronounced when examined 8 weeks after TAC, albeit hearts from MK2−/− mice after 8-week TAC showed a better compliance. These differences suggest that rather than abrogating pressure overload–induced contractile dysfunction, the absence of MK2 delays the pathogenic response. MK5 is a putative target of p38α/β as well as atypical MAP kinases ERK3 and ERK4 that is also expressed in heart cells.[94,95] In contrast to the effects shown herein for MK2 deficiency, MK5 haplodeficiency results in a significant attenuation of LV hypertrophy 8 weeks after TAC.[40] The downstream effectors of MK2 and MK5 in cardiac cells and their roles in pathological remodeling of the myocardium remain to be determined.

Potential Limitations

One limitation of the present study is the animal model. The MK2-deficient mice are pan knockouts rather than cardiomyocyte specific. Hence, the involvement of body temperature, peripheral mechanisms, or systemic mediators in the observed cardiac phenotype cannot be excluded. In addition, although the overall aim of this study was to perform a comprehensive analysis of the role of MK2 in regulating basal cardiac function and its implication in pathological remodeling, our results do not shed light on the molecular mechanisms by which MK2 regulates cardiac function in health and disease, thereby representing another limitation. Further studies using cell type–specific MK2-deficient models will be required.

CONCLUSIONS

MK2-deficient mice showed no adverse effects on myocardial performance over time. Interestingly, autonomic regulation of cardiac function appears to be altered in the absence of MK2. In addition, MK2-deficient mice showed changes in the expression of some metabolic genes related to mitochondrial biogenesis and fatty acid metabolism, despite no alterations in mitochondrial respiration rates. Furthermore, the calcium-sensitivity for mPTP opening was reduced, suggesting a cardioprotective effect of MK2 loss. Finally, in response to a chronic increase in afterload, LV hypertrophy was delayed but not reduced or prevented. Altogether these findings support a novel role for MK2 in the heart that merits

further investigation, especially in regard to its possible role in autonomic regulation of heart function, the regulation of metabolic gene expression, and mPTP opening as these may represent interesting cardioprotective roles for inhibitors of MK2. In addition, consistent with previous work using a constitutive form of MK2 deficiency, we confirm that MK2 is implicated in the pathological processes leading to cardiac hypertrophy and ventricular dysfunction.

ARTICLE INFORMATION

Affiliations

From the Department of Medicine (M.R., J.-C.T., B.G.A.), Department of Biochemistry and Molecular Medicine (M.K., D.D., G.V., J.T., P.S., B.G.A.), Department of Pharmacology and Physiology (S.A.N., A.N., M.G.S., B.G.A.), and Faculté de Pharmacie (S.T., C.F.), Université de Montréal, Québec, Canada; Montreal Heart Institute, Montréal, Québec, Canada (M.R., M.K., D.D., G.V., S.T., J.T., Y.S., A.D., B.H., S.A.N., P.S., A.N., F.S., M.-A.G., M.G.S., C.F., J.-C.T., B.G.A.); University of Maryland, Baltimore, MD (R.J.K., W.C.S.); L'Institut du Thorax, INSERM, CNRS, Université de Nantes, France (B.L.); Institute of Cell Biochemistry, Hannover Medical School, Hannover, Germany (M.G.); and Department of Physiology, Faculty of Medicine, Suez Canal University, Ismailia, Egypt (S.A.N.).

Acknowledgments

Sources of Funding

Disclosures

None.

REFERENCES

1. Frey N, Katus HA, Olson EN, Hill JA. Hypertrophy of the heart: a new therapeutic target? *Circulation*. 2004;109:1580–1589. DOI:10.1161/01. CIR.0000120390.68287.BB.

2. Depre C, Shipley GL, Chen W, Han Q, Doenst T, Moore ML, Stepkowski S, Davies PJ, Taegtmeyer H. Unloaded heart in vivo replicates fetal gene expression of cardiac hypertrophy. *Nat Med*. 1998;4:1269–1275. DOI:10.1038/3253.

3. Kong P, Christia P, Frangogiannis NG. The pathogenesis of cardiac fibrosis. *Cell Mol Life Sci*. 2014;71:549–574. DOI:10.1007/s00018-013-1349-6.

4. Sadoshima J, Izumo S. The cellular and molecular response of cardiac myocytes to mechanical stress. *Annu Rev Physiol*. 1997;59:551–571. DOI:10.1146/annurev.physiol.59.1.551.

5. Frey N, Luedde M, Katus HA. Mechanisms of disease: hypertrophic cardiomyopathy. *Nat Rev Cardiol*. 2011;9:91–100. DOI:10.1038/nrcardio.2011.159.

6. Shah AM, Mann DL. In search of new therapeutic targets and strategies for heart failure: recent advances in basic science. *Lancet*. 2011;378:704–712. DOI:10.1016/S0140-6736(11)60894-5.

7. Trempolec N, Dave-Coll N, Nebreda AR. SnapShot: p38 MAPK signaling. *Cell*. 2013;152:656–656.e1. DOI:10.1016/j.cell.2013.01.029.

8. Arabacilar P, Marber M. The case for inhibiting p38 mitogen-activated protein kinase in heart failure. *Front Pharmacol*. 2015;6:102. DOI:10.3389/fphar.2015.00102.

9. Bellahcene M, Jacquet S, Cao XB, Tanno M, Haworth RS, Layland J, Kabir AM, Gaestel M, Davis RJ, Flavell RA, et al. Activation of p38 mitogen-activated protein kinase contributes to the early cardiodepressant action of tumor necrosis factor. *J Am Coll Cardiol*. 2006;48:545–555. DOI:10.1016/j.jacc.2006.02.072.

10. Chahine MN, Mioulane M, Sikkel MB, O'Gara P, Dos Remedios CG, Pierce GN, Lyon AR, Foldes G, Harding SE. Nuclear pore rearrangements and nuclear trafficking in cardiomyocytes from rat and human failing hearts. *Cardiovasc Res*. 2015;105:31–43. DOI:10.1093/cvr/cvu218.

11. Takeishi Y, Huang Q, Abe J, Che W, Lee JD, Kawakatsu H, Hoit BD, Berk BC, Walsh RA. Activation of mitogen-activated protein kinases and p90 ribosomal S6 kinase in failing human hearts with dilated cardiomyopathy. *Cardiovasc Res*. 2002;53:131–137. DOI:10.1016/S0008-6363(01)00438-2.

12. Dingar D, Merlen C, Grandy S, Gillis MA, Villeneuve LR, Mamarbachi AM, Fiset C, Allen BG. Effect of pressure overload-induced hypertrophy on the expression and localization of p38 MAP kinase isoforms in the mouse heart. *Cell Signal*. 2010;22:1634–1644. DOI:10.1016/j.cellsig.2010.06.002.

13. Lemke LE, Bloem LJ, Fouts R, Esterman M, Sandusky G, Vlahos CJ. Decreased p38 MAPK activity in end-stage failing human myocardium: p38 MAPK is the predominant isoform expressed in human heart. *J Mol Cell Cardiol*. 2001;33:1527–1540.

14. Wang Y, Huang S, Sah VP, Ross J Jr, Brown JH, Han J, Chien KR. Cardiac muscle cell hypertrophy and apoptosis induced by distinct members of the p38 mitogen-activated protein kinase family. *J Biol Chem*. 1998;273:2161–2168.

15. Yokota T, Wang Y. p38 MAP kinases in the heart. *Gene*. 2016;575:369–376. DOI:10.1016/j.gene.2015.09.030.

16. Gonzalez-Teran B, Lopez JA, Rodriguez E, Leiva L, Martinez-Martinez S, Bernal JA, Jimenez-Borreguero LJ, Redondo JM, Vazquez J, Sabio G. p38γ and δ promote heart hypertrophy by targeting the mTOR-inhibitory protein DEPTOR for degradation. *Nat Commun*. 2016;7:10477. DOI:10.1038/ncomms10477.

17. Nemoto S, Sheng Z, Lin A. Opposing effects of Jun kinase and p38 mitogen-activated protein kinases on cardiomyocyte hypertrophy. *Mol Cell Biol*. 1998;18:3518–3526.

18. Braz JC, Bueno OF, Liang Q, Wilkins BJ, Dai Y-S, Parsons S, Braunwart J, Glascock BJ, Klevitsky R, Kimball TF, et al. Targeted inhibition of p38 MAPK promotes hypertrophic cardiomyopathy through upregulation of calcineurin-NFAT signaling. *J Clin Invest*. 2003;111:1475–1486. DOI:10.1172/JCI200317295.

19. Zhang S, Weinheimer C, Courtois M, Kovacs A, Zhang CE, Cheng AM, Wang Y, Muslin AJ. The role of the Grb2-p38 MAPK signaling pathway in cardiac hypertrophy and fibrosis. *J Clin Invest*. 2003;111:833–841. DOI:10.1172/JCI16290.

20. Nishida K, Yamaguchi O, Hirotani S, Hikoso S, Higuchi Y, Watanabe T, Takeda T, Osuka S, Morita T, Kondoh G, et al. p38α mitogen-activated protein kinase plays a critical role in cardiomyocyte survival but not in cardiac hypertrophic growth in response to pressure overload. *Mol Cell Biol*. 2004;24:10611–10620.

21. Streicher JM, Ren S, Herschman H, Wang Y. MAPK-activated protein kinase-2 in cardiac hypertrophy and cyclooxygenase-2 regulation in heart. *Circ Res*. 2010;106:1434–1443.

22. Cargnello M, Roux PP. Activation and function of the MAPKs and their substrates, the MAPK-activated protein kinases. *Microbiol Mol Biol Rev*. 2011;75:50–83. DOI:10.1128/MMBR.00031-10.

23. Coulthard LR, White DE, Jones DL, McDermott MF, Burchill SA. p38MAPK: stress responses from molecular mechanisms to therapeutics. *Trends Mol Med*. 2009;15:369–379. DOI:10.1016/j.molmed.2009.06.005.

24. Marber MS, Rose B, Wang Y. The p38 mitogen-activated protein kinase pathway—a potential target for intervention in infarction, hypertrophy,

and heart failure. *J Mol Cell Cardiol*. 2011;51:485–490. DOI:10.1016/j.yjmcc.2010.10.021.

25. Martin ED, Bassi R, Marber MS. p38 MAPK in cardioprotection—are we there yet? *Br J Pharmacol*. 2015;172:2101–2113. DOI:10.1111/bph.12901.

26. Fiore M, Forli S, Manetti F. Targeting mitogen-activated protein kinase-activated protein kinase 2 (MAPKAPK2, MK2): medicinal chemistry efforts to lead small molecule inhibitors to clinical trials. *J Med Chem*. 2016;59:3609–3634. DOI:10.1021/acs.jmedchem.5b01457.

27. Arthur JS, Ley SC. Mitogen-activated protein kinases in innate immunity. *Nat Rev Immunol*. 2013;13:679–692. DOI:10.1038/nri3495.

28. Cheung PC, Campbell DG, Nebreda AR, Cohen P. Feedback control of the protein kinase TAK1 by SAPK2a/p38α. *EMBO J*. 2003;22:5793–5805. DOI:10.1093/emboj/cdg552.

29. Dulos J, Wijnands FP, van den Hurk-van Alebeek JA, van Vugt MJ, Rullmann JA, Schot JJ, de Groot MW, Wagenaars JL, van Ravestein-van OR, Smets RL, et al. p38 inhibition and not MK2 inhibition enhances the secretion of chemokines from TNF-α activated rheumatoid arthritis fibroblast-like synoviocytes. *Clin Exp Rheumatol*. 2013;31:515–525.

30. Ruiz M, Coderre L, Allen BG, Des RC. Protecting the heart through MK2 modulation, toward a role in diabetic cardiomyopathy and lipid metabolism. *Biochim Biophys Acta*. 2018;1864:1914–1922. DOI:10.1016/j.bbadis.2017.07.015.

31. Shiroto K, Otani H, Yamamoto F, Huang CK, Maulik N, Das DK. MK2$^{-/-}$ gene knockout mouse hearts carry anti-apoptotic signal and are resistant to ischemia reperfusion injury. *J Mol Cell Cardiol*. 2005;38:93–97.

32. Xu L, Yates CC, Lockyer P, Xie L, Bevilacqua A, He J, Lander C, Patterson C, Willis M. MMI-0100 inhibits cardiac fibrosis in myocardial infarction by direct actions on cardiomyocytes and fibroblasts via MK2 inhibition. *J Mol Cell Cardiol*. 2014;77:86–101. DOI:10.1016/j.yjmcc.2014.09.011.

33. Ruiz M, Coderre L, Lachance D, Houde V, Martel C, Thompson Legault J, Gillis M-A, Bouchard B, Daneault C, Carpentier AC, et al. MK2 deletion in mice prevents diabetes-induced perturbations in lipid metabolism and cardiac dysfunction. *Diabetes*. 2016;65:381–392. DOI:10.2337/db15-0238.

34. Kotlyarov A, Neininger A, Schubert C, Eckert R, Birchmeier C, Volk H-D, Gaestel M. MAPKAP kinase-2 is essential for LPS-induced TNF-α biosynthesis. *Nat Cell Biol*. 1999;1:94–97. DOI:10.1038/10061.

35. Brouillette J, Grandy SA, Jolicoeur P, Fiset C. Cardiac repolarization is prolonged in CD4C/HIV transgenic mice. *J Mol Cell Cardiol*. 2007;43:159–167. DOI:10.1016/j.yjmcc.2007.05.007.

36. Mitchell GF, Jeron A, Koren G. Measurement of heart rate and Q-T interval in the conscious mouse. *Am J Physiol*. 1998;274:H747–H751. DOI:10.1152/ajpheart.1998.274.3.H747.

37. Shaffer F, Ginsberg JP. An overview of heart rate variability metrics and norms. *Front Public Health*. 2017;5:258. DOI:10.3389/fpubh.2017.00258.

38. El Khoury N, Mathieu S, Marger L, Ross J, El Gebeily G, Ethier N, Fiset C. Upregulation of the hyperpolarization-activated current increases pacemaker activity of the sinoatrial node and heart rate during pregnancy in mice. *Circulation*. 2013;127:2009–2020. DOI:10.1161/CIRCULATIONAHA.113.001683.

39. Merlet N, Busseuil D, Mihalache-Avram T, Mecteau M, Shi Y, Nachar W, Brand G, Brodeur MR, Charpentier D, Rhainds D, et al. HDL mimetic peptide CER-522 treatment regresses left ventricular diastolic dysfunction in cholesterol-fed rabbits. *Int J Cardiol*. 2016;215:364–371. DOI:10.1016/j.ijcard.2016.04.029.

40. Nawaito SA, Dingar D, Sahadevan P, Hussein B, Sahmi F, Shi Y, Gillis MA, Gaestel M, Tardif JC, Allen BG. MK5 haplodeficiency attenuates hypertrophy and preserves diastolic function during remodeling induced by chronic pressure overload in the mouse heart. *Am J Physiol Heart Circ Physiol*. 2017;313:H46–H58. DOI:10.1152/ajpheart.00597.2016.

41. Nawaito SA, Sahadevan P, Clavet-Lanthier M-É, Pouliot P, Sahmi F, Shi Y, Gillis M-A, Lesage F, Gaestel M, Sirois MG, et al. MK5 haplodeficiency decreases collagen deposition and scar size during post-myocardial infarction wound repair. *Am J Physiol Heart Circ Physiol*. 2019;316:H1281–H1296. DOI:10.1152/ajpheart.00532.2017.

42. Khairallah M, Labarthe F, Bouchard B, Danialou G, Petrof BJ, Des RC. Profiling substrate fluxes in the isolated working mouse heart using ^{13}C-labeled substrates: focusing on the origin and fate of pyruvate and citrate carbons. *Am J Physiol*. 2004;286:H1461–H1470.

43. Rivard K, Grandy SA, Douillette A, Paradis P, Nemer M, Allen BG, Fiset C. Overexpression of type 1 angiotensin II receptors impairs excitation-contraction coupling in the mouse heart. *Am J Physiol Heart Circ Physiol*. 2011;301:H2018–H2027. DOI:10.1152/ajpheart.01092.2010.

44. Khairallah RJ, Sparagna GC, Khanna N, O'Shea KM, Hecker PA, Kristian T, Fiskum G, Des Rosiers C, Polster BM, Stanley WC. Dietary supplementation with docosahexaenoic acid, but not eicosapentaenoic acid, dramatically alters cardiac mitochondrial phospholipid fatty acid composition and prevents permeability transition. *Biochim Biophys Acta*. 2010;1797:1555–1562.

45. O'Shea KM, Khairallah RJ, Sparagna GC, Xu W, Hecker PA, Robillard-Frayne I, Des Rosiers C, Kristian T, Murphy RC, Fiskum G, et al. Dietary omega-3 fatty acids alter cardiac mitochondrial phospholipid composition and delay Ca^{2+}-induced permeability transition. *J Mol Cell Cardiol*. 2009;47:819–827.

46. Khairallah RJ, O'Shea KM, Brown BH, Khanna N, Des Rosiers C, Stanley WC. Treatment with docosahexaenoic acid, but not eicosapentaenoic acid, delays Ca^{2+}-induced mitochondria permeability transition in normal and hypertrophied myocardium. *J Pharmacol Exp Ther*. 2010;335:155–162.

47. Gelinas R, Labarthe F, Bouchard B, Mc Duff J, Charron G, Young ME, Des RC. Alterations in carbohydrate metabolism and its regulation in PPARalpha null mouse hearts. *Am J Physiol Heart Circ Physiol*. 2008;294:H1571–H1580.

48. Nawaito SA, Sahadevan P, Sahmi F, Gaestel M, Calderone A, Allen BG. Transcript levels for extracellular matrix proteins are altered in MK5-deficient cardiac ventricular fibroblasts. *J Mol Cell Cardiol*. 2019;132:164–177. DOI:10.1016/j.yjmcc.2019.05.014.

49. Duda MK, O'Shea KM, Tintinu A, Xu W, Khairallah RJ, Barrows BR, Chess DJ, Azimzadeh AM, Harris WS, Sharov VG, et al. Fish oil, but not flaxseed oil, decreases inflammation and prevents pressure overload-induced cardiac dysfunction. *Cardiovasc Res*. 2009;81:319–327. DOI:10.1093/cvr/cvn310.

50. Connern CP, Halestrap AP. Chaotropic agents and increased matrix volume enhance binding of mitochondrial cyclophilin to the inner mitochondrial membrane and sensitize the mitochondrial permeability transition to [Ca^{2+}]. *Biochemistry*. 1996;35:8172–8180.

51. Trulley P, Snieckute G, Bekker-Jensen D, Menon MB, Freund R, Kotlyarov A, Olsen JV, Diaz-Muñoz MD, Turner M, Bekker-Jensen S, et al. Alternative translation initiation generates a functionally distinct isoform of the stress-activated protein kinase MK2. *Cell Rep*. 2019;27:2859–2870.e2856. DOI:10.1016/j.celrep.2019.05.024.

52. Kaul S, Tei C, Hopkins JM, Shah PM. Assessment of right ventricular function using two-dimensional echocardiography. *Am Heart J*. 1984;107:526–531. DOI:10.1016/0002-8703(84)90095-4.

53. Constantinides C, Murphy K. Molecular and integrative physiological effects of isoflurane anesthesia: the paradigm of cardiovascular studies in rodents using magnetic resonance imaging. *Front Cardiovasc Med*. 2016;3:23. DOI:10.3389/fcvm.2016.00023.

54. Verweij N, Mateo Leach I, van den Boogaard M, van Veldhuisen DJ, Christoffels VM; LifeLines Cohort S, Hillege HL, van Gilst WH, Barnett P, de Boer RA, van der Harst P. Genetic determinants of P wave duration and PR segment. *Circ Cardiovasc Genet*. 2014;7:475–481. DOI:10.1161/CIRCGENETICS.113.000373.

55. Esposito G, Prasad SVN, Rapacciuolo A, Mao L, Koch WJ, Rockman HA. Cardiac overexpression of a Gq inhibitor blocks induction of extracellular signal–regulated kinase and c-Jun NH$_2$-terminal kinase activity in in vivo pressure overload. *Circulation*. 2001;103:1453–1458.

56. Akashi YJ, Springer J, Lainscak M, Anker SD. Atrial natriuretic peptide and related peptides. *Clin Chem Lab Med*. 2007;45:1259–1267.

57. Abhayaratna WP, Seward JB, Appleton CP, Douglas PS, Oh JK, Tajik AJ, Tsang TS. Left atrial size: physiologic determinants and clinical applications. *J Am Coll Cardiol*. 2006;47:2357–2363. DOI:10.1016/j.jacc.2006.02.048.

58. Boivin B, Allen BG. p38 MAP kinase attenuates phorbol ester-induced ERK MAP kinase activation in adult cardiac ventricular myocytes. *Curr Top Biochem Res*. 2012;14:57–63.

59. Kotlyarov A, Yannoni Y, Fritz S, Laaß T-B, Pitman D, Lin L-L, Gaestel M. Distinct cellular functions of MK2. *Mol Cell Biol*. 2002;22:4827–4835.

60. Fukuta H, Little WC. The cardiac cycle and the physiologic basis of left ventricular contraction, ejection, relaxation, and filling. *Heart Fail Clin*. 2008;4:1–11. DOI:10.1016/j.hfc.2007.10.004.

61. Nakou ES, Parthenakis FI, Kallergis EM, Marketou ME, Nakos KS, Vardas PE. Healthy aging and myocardium: a complicated process with various effects in cardiac structure and physiology. *Int J Cardiol.* 2016;209:167–175. DOI:10.1016/j.ijcard.2016.02.039.

62. Esfandiari S, Fuchs F, Wainstein RV, Chelvanathan A, Mitoff P, Sasson Z, Mak S. Heart rate-dependent left ventricular diastolic function in patients with and without heart failure. *J Card Fail.* 2015;21:68–75. DOI:10.1016/j.cardfail.2014.10.013.

63. Ha JW, Oh JK. Therapeutic strategies for diastolic dysfunction: a clinical perspective. *J Cardiovasc Ultrasound.* 2009;17:86–95. DOI:10.4250/jcu.2009.17.3.86.

64. Gordan R, Gwathmey JK, Xie LH. Autonomic and endocrine control of cardiovascular function. *World J Cardiol.* 2015;7:204–214. DOI:10.4330/wjc.v7.i4.204.

65. Salazar NC, Chen J, Rockman HA. Cardiac GPCRs: GPCR signaling in healthy and failing hearts. *Biochim Biophys Acta.* 2007;1768:1006–1018. DOI:10.1016/j.bbamem.2007.02.010.

66. Dorn GW II, Vega RB, Kelly DP. Mitochondrial biogenesis and dynamics in the developing and diseased heart. *Genes Dev.* 2015;29:1981–1991. DOI:10.1101/gad.269894.115.

67. Arany Z, Novikov M, Chin S, Ma Y, Rosenzweig A, Spiegelman BM. Transverse aortic constriction leads to accelerated heart failure in mice lacking PPAR-γ coactivator 1α. *Proc Natl Acad Sci U S A.* 2006;103:10086–10091.

68. Riehle C, Wende AR, Zaha VG, Pires KM, Wayment B, Olsen C, Bugger H, Buchanan J, Wang X, Moreira AB, et al. PGC-1β deficiency accelerates the transition to heart failure in pressure overload hypertrophy. *Circ Res.* 2011;109:783–793. DOI:10.1161/CIRCRESAHA.111.243964.

69. Lai L, Leone TC, Zechner C, Schaeffer PJ, Kelly SM, Flanagan DP, Medeiros DM, Kovacs A, Kelly DP. Transcriptional coactivators PGC-1α and PGC-lβ control overlapping programs required for perinatal maturation of the heart. *Genes Dev.* 2008;22:1948–1961.

70. Faerber G, Barreto-Perreia F, Schoepe M, Gilsbach R, Schrepper A, Schwarzer M, Mohr FW, Hein L, Doenst T. Induction of heart failure by minimally invasive aortic constriction in mice: reduced peroxisome proliferator-activated receptor γ coactivator levels and mitochondrial dysfunction. *J Thorac Cardiovasc Surg.* 2011;141:492–500.

71. Garnier A, Fortin D, Delomenie C, Momken I, Veksler V, Ventura-Clapier R. Depressed mitochondrial transcription factors and oxidative capacity in rat failing cardiac and skeletal muscles. *J Physiol.* 2003;551:491–501. DOI:10.1113/jphysiol.2003.045104.

72. Sebastiani M, Giordano C, Nediani C, Travaglini C, Borchi E, Zani M, Feccia M, Mancini M, Petrozza V, Cossarizza A, et al. Induction of mitochondrial biogenesis is a maladaptive mechanism in mitochondrial cardiomyopathies. *J Am Coll Cardiol.* 2007;50:1362–1369. DOI:10.1016/j.jacc.2007.06.035.

73. Lee WS, Kim J. Peroxisome proliferator-activated receptors and the heart: lessons from the past and future directions. *PPAR Res.* 2015;2015:271983.

74. Neubauer S. The failing heart—an engine out of fuel. *N Engl J Med.* 2007;356:1140–1151. DOI:10.1056/NEJMra063052.

75. Bayeva M, Gheorghiade M, Ardehali H. Mitochondria as a therapeutic target in heart failure. *J Am Coll Cardiol.* 2013;61:599–610. DOI:10.1016/j.jacc.2012.08.1021.

76. Neininger A, Kontoyiannis D, Kotlyarov A, Winzen R, Eckert R, Volk HD, Holtmann H, Kollias G, Gaestel M. MK2 targets AU-rich elements and regulates biosynthesis of tumor necrosis factor and interleukin-6 independently at different post-transcriptional levels. *J Biol Chem.* 2002;277:3065–3068.

77. Scharf M, Neef S, Freund R, Geers-Knorr C, Franz-Wachtel M, Brandis A, Krone D, Schneider H, Groos S, Menon MB, et al. Mitogen-activated protein kinase-activated protein kinases 2 and 3 regulate SERCA2a expression and fiber type composition to modulate skeletal muscle and cardiomyocyte function. *Mol Cell Biol.* 2013;33:2586–2602. DOI:10.1128/MCB.01692-12.

78. Akhmedov AT, Rybin V, Marin-Garcia J. Mitochondrial oxidative metabolism and uncoupling proteins in the failing heart. *Heart Fail Rev.* 2015;20:227–249. DOI:10.1007/s10741-014-9457-4.

79. Laskowski KR, Russell RR III. Uncoupling proteins in heart failure. *Curr Heart Fail Rep.* 2008;5:75–79. DOI:10.1007/s11897-008-0013-1.

80. Murray AJ, Cole MA, Lygate CA, Carr CA, Stuckey DJ, Little SE, Neubauer S, Clarke K. Increased mitochondrial uncoupling proteins, respiratory uncoupling and decreased efficiency in the chronically infarcted rat heart. *J Mol Cell Cardiol.* 2008;44:694–700. DOI:10.1016/j.yjmcc.2008.01.008.

81. Rial E, Rodriguez-Sanchez L, Gallardo-Vara E, Zaragoza P, Moyano E, Gonzalez-Barroso MM. Lipotoxicity, fatty acid uncoupling and mitochondrial carrier function. *Biochim Biophys Acta.* 2010;1797:800–806. DOI:10.1016/j.bbabio.2010.04.001.

82. Kwong JQ, Molkentin JD. Physiological and pathological roles of the mitochondrial permeability transition pore in the heart. *Cell Metab.* 2015;21:206–214. DOI:10.1016/j.cmet.2014.12.001.

83. Perez MJ, Quintanilla RA. Development or disease: duality of the mitochondrial permeability transition pore. *Dev Biol.* 2017;426:1–7. DOI:10.1016/j.ydbio.2017.04.018.

84. Bernardi P, Di Lisa F. The mitochondrial permeability transition pore: molecular nature and role as a target in cardioprotection. *J Mol Cell Cardiol.* 2015;78:100–106. DOI:10.1016/j.yjmcc.2014.09.023.

85. Kinnally KW, Peixoto PM, Ryu SY, Dejean LM. Is mPTP the gatekeeper for necrosis, apoptosis, or both? *Biochim Biophys Acta.* 2011;1813:616–622. DOI:10.1016/j.bbamcr.2010.09.013.

86. Di Lisa F, Menabo R, Canton M, Barile M, Bernardi P. Opening of the mitochondrial permeability transition pore causes depletion of mitochondrial and cytosolic NAD+ and is a causative event in the death of myocytes in postischemic reperfusion of the heart. *J Biol Chem.* 2001;276:2571–2575.

87. Marcil M, Ascah A, Matas J, Bélanger S, Deschepper CF, Burelle Y. Compensated volume overload increases the vulnerability of heart mitochondria without affecting their functions in the absence of stress. *J Mol Cell Cardiol.* 2006;41:998–1009. DOI:10.1016/j.yjmcc.2006.08.117.

88. Matas J, Young NT, Bourcier-Lucas C, Ascah A, Marcil M, Deschepper CF, Burelle Y. Increased expression and intramitochondrial translocation of cyclophilin-D associates with increased vulnerability of the permeability transition pore to stress-induced opening during compensated ventricular hypertrophy. *J Mol Cell Cardiol.* 2009;46:420–430. DOI:10.1016/j.yjmcc.2008.10.020.

89. Javadov S, Huang C, Kirshenbaum L, Karmazyn M. NHE-1 inhibition improves impaired mitochondrial permeability transition and respiratory function during postinfarction remodelling in the rat. *J Mol Cell Cardiol.* 2005;38:135–143. DOI:10.1016/j.yjmcc.2004.10.007.

90. Sharov VG, Todor A, Khanal S, Imai M, Sabbah HN. Cyclosporine A attenuates mitochondrial permeability transition and improves mitochondrial respiratory function in cardiomyocytes isolated from dogs with heart failure. *J Mol Cell Cardiol.* 2007;42:150–158. DOI:10.1016/j.yjmcc.2006.09.013.

91. Dabkowski ER, O'Connell KA, Xu W, Ribeiro RF Jr, Hecker PA, Shekar KC, Daneault C, Des Rosiers C, Stanley WC. Docosahexaenoic acid supplementation alters key properties of cardiac mitochondria and modestly attenuates development of left ventricular dysfunction in pressure overload-induced heart failure. *Cardiovasc Drugs Ther.* 2013;27:499–510. DOI:10.1007/s10557-013-6487-4.

92. Javadov S, Karmazyn M, Escobales N. Mitochondrial permeability transition pore opening as a promising therapeutic target in cardiac diseases. *J Pharmacol Exp Ther.* 2009;330:670–678. DOI:10.1124/jpet.109.153213.

93. Clements RT, Feng J, Cordeiro B, Bianchi C, Sellke FW. p38 MAPK-dependent small HSP27 and αB-crystallin phosphorylation in regulation of myocardial function following cardioplegic arrest. *Am J Physiol Heart Circ Physiol.* 2011;300:H1669–H1677. DOI:10.1152/ajpheart.00272.2010.

94. Dingar D, Benoit MJ, Mamarbachi AM, Villeneuve LR, Gillis MA, Grandy S, Gaestel M, Fiset C, Allen BG. Characterization of the expression and regulation of MK5 in the murine ventricular myocardium. *Cell Signal.* 2010;22:1063–1075. DOI:10.1016/j.cellsig.2010.02.009.

95. Sahadevan P, Allen BG. MK5: a novel regulator of cardiac fibroblast function? *IUBMB Life.* 2017;69:785–794. DOI:10.1002/iub.1677.